HHS Public Access

Author manuscript

Cell Rep. Author manuscript; available in PMC 2021 September 24.

Published in final edited form as:

Cell Rep. 2021 September 07; 36(10): 109666. doi:10.1016/j.celrep.2021.109666.

Topoisomerase I inhibition and peripheral nerve injury induce DNA breaks and ATF3-associated axon regeneration in sensory neurons

Yung-Chih Cheng[1,2], **Andrew Snavely**[1,2], **Lee B. Barrett**[1,2], **Xuefei Zhang**[7,8,9,10], **Crystal Herman**[1], **Devlin J. Frost**[1], **Priscilla Riva**[1], **Ivan Tochitsky**[1,2], **Riki Kawaguchi**[6], **Bhagat Singh**[1,2], **Jelena Ivanis**[1], **Eric A. Huebner**[1,2], **Anthony Arvanites**[4], **Vatsal Oza**[4], **Lance Davidow**[4], **Rie Maeda**[1], **Miyuki Sakuma**[1,2], **Alyssa Grantham**[1], **Qing Wang**[6], **Amelia N. Chang**[7,8,9], **Kathleen Pfaff**[4], **Michael Costigan**[1,5], **Giovanni Coppola**[6], **Lee L. Rubin**[3,4], **Bjoern Schwer**[7,8,9,11], **Frederick W. Alt**[7,8,9], **Clifford J. Woolf**[1,2,4,12,*]

[1]F.M. Kirby Neurobiology Center, Program in Neurobiology, Boston Children's Hospital, Boston, MA 02115, USA

[2]Department of Neurobiology, Harvard Medical School, Boston, MA 02115, USA

[3]Department of Stem Cell and Regenerative Biology, Harvard University, Cambridge, MA 02138, USA

[4]Harvard Stem Cell Institute, Harvard University, Cambridge, MA 02138, USA

[5]Anaesthesia Department, Boston Children's Hospital, Boston, MA 02115, USA

[6]Departments of Psychiatry and Neurology, Semel Institute for Neuroscience and Human Behavior, David Geffen School of Medicine, University of California, Los Angeles, CA 90095, USA

[7]Program in Cellular and Molecular Medicine, Boston Children's Hospital, Howard Hughes Medical Institute, Boston, MA 02115, USA

[8]Department of Genetics, Harvard Medical School, Boston, MA 02115, USA

[9]Department of Pediatrics, Harvard Medical School, Boston, MA 02115, USA

[*]Correspondence: clifford.woolf@childrens.harvard.edu.

AUTHOR CONTRIBUTIONS

Conceptualization, Y.-C.C. and C.J.W.; methodology, Y.-C.C., A.S., X.Z., B. Schwer, A.A., L.D., K.P., L.L.R., A.N.C., F.W.A., and C.J.W.; investigation, Y.-C.C., A.S., R.K., Q.W., P.R., C.H., D.J.F., B. Singh, I.T., V.O., L.B.B., X.Z., M.C., M.S., J.I., A.G., R.M., and E.H.; writing-original draft, Y.-C.C., A.S., and C.J.W.; writing-review & editing, Y.-C.C., A.S., X.Z., G.C., L.L.R., B. Schwer, F.W.A., and C.J.W.; funding acquisition, C.J.W.; resources, G.C., L.L.R., and F.A.; supervision, Y.-C. C. and C.J.W.

SUPPLEMENTAL INFORMATION

Supplemental information can be found online at https://doi.org/10.1016/j.celrep.2021.109666.

DECLARATION OF INTERESTS

Y.-C.C. is a current employee of Pfizer. P.R. is a current employee of Biogen. I.T. and G.C. are current employees of Regeneron. B. Singh is a current employee of Takeda. A.A. is a current employee of HotSpot Therapeutics. V.O. is a current employee of Amgen. R.M. and A.G. are current employees of Novartis. C.J.W. is a founder of Nocion Therapeutics and QurAlis and a SAB member of Enclear Therapeutics and Cygnal Therapeutics.

[10]Present address: Biomedical Pioneering Innovation Center (BIOPIC) and Beijing Advanced Innovation Center for Genomics (ICG), Peking University, Beijing 100871, China

[11]Present address: The Eli and Edythe Broad Center of Regeneration Medicine and Stem Cell Research, Bakar Aging Research Institute, Kavli Institute for Fundamental Neuroscience, Department of Neurological Surgery, University of California, San Francisco, San Francisco, CA 94143, USA

[12]Lead contact

SUMMARY

Although axonal damage induces rapid changes in gene expression in primary sensory neurons, it remains unclear how this process is initiated. The transcription factor ATF3, one of the earliest genes responding to nerve injury, regulates expression of downstream genes that enable axon regeneration. By exploiting ATF3 reporter systems, we identify topoisomerase inhibitors as ATF3 inducers, including camptothecin. Camptothecin increases ATF3 expression and promotes neurite outgrowth in sensory neurons *in vitro* and enhances axonal regeneration after sciatic nerve crush *in vivo.* Given the action of topoisomerases in producing DNA breaks, we determine that they do occur immediately after nerve damage at the ATF3 gene locus in injured sensory neurons and are further increased after camptothecin exposure. Formation of DNA breaks in injured sensory neurons and enhancement of it pharmacologically may contribute to the initiation of those transcriptional changes required for peripheral nerve regeneration.

Graphical abstract

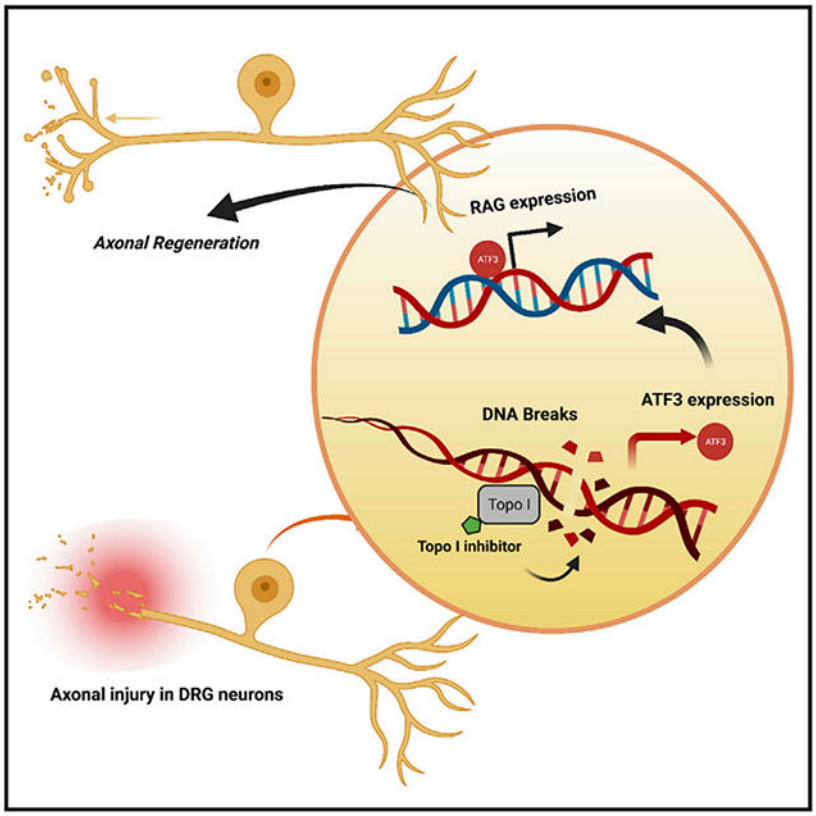

In brief

Sensory neurons induce regeneration-associated genes after injury in an ATF3-dependent manner, enabling axonal regeneration. Cheng et al. use an ATF3 reporter screen to identify Topo I inhibition as an ATF3 inducer and regeneration promotor. Nerve injury rapidly causes DNA breaks at the ATF3 locus, which are increased by Topo I inhibition.

INTRODUCTION

Regeneration of sensory and motor neurons after injury to their peripheral axons is enabled by expression of a large set of regeneration-associated genes (RAGs) that provide the molecular machinery necessary for axonal formation, elongation, and guidance (Chandran et al., 2016; Mar et al., 2014; Renthal et al., 2020). Expression of the RAG gene set is accomplished by activation of several signaling pathways in the cell soma after axonal damage (Chan et al., 2014), leading to the expression and phosphorylation of a broad number of transcription factors (Moore et al., 2009), including c-JUN (Raivich et al., 2004), STAT3 (Lee et al., 2004), SOX11 (Jankowski et al., 2006), SMAD1 (Okuyama et al., 2007), and ATF3 (Huang et al., 2006; Renthal et al., 2020). Involvement of these transcription factors as “master regulators” of the regeneration transcriptional network is confirmed by impairment of peripheral nervous system (PNS) regeneration after their deletion or depletion, as for c-JUN or SMAD1 (Saijilafu et al., 2013) or ATF3 (Renthal et al., 2020), and by the increased axonal growth in the CNS and PNS following forced overexpression or

activation of c-JUN, SMAD1, SOX11, or ATF3 (Chandran et al., 2016; Fagoe et al., 2015; Huang et al., 2015; Seijffers et al., 2006; Wang et al., 2015).

ATF3, a member of the ATF/CREB family of transcription factors (Hai and Hartman, 2001), is the most highly induced transcription factor in successfully regenerating dorsal root ganglion (DRG) sensory neurons (Li et al., 2015; Renthal et al., 2020), and because it appears to be universally expressed in injured DRG neurons, ATF3 is commonly used as a marker of axonal injury (Lindå et al., 2011; Tsujino et al., 2000). ATF3 is also activated in a number of different cell types by stress (Hai et al., 1999), as well as by cancer chemotherapeutic drugs, proteasome inhibitors, and genotoxic agents (Kool et al., 2003). ATF3 interacts with a number of other transcription factors, including c-JUN, to form a complex that can either repress or activate various genes (Thompson et al., 2009). The induction of ATF3 and c-JUN appears to be a major driver of the gene expression program necessary for increased axonal growth (Campbell et al., 2005; Chandran et al., 2016; Huang et al., 2015; Renthal et al., 2020; Seijffers et al., 2007).

Although, how multiple transcriptional factor master regulators are rapidly induced by axonal injury to drive the regeneration gene network is unclear. Calcium influx into the axoplasm is one of the first signals induced by nerve injury, and a back-propagating calcium wave from the injured axon invades the soma causing protein kinase C (PKC) activation followed by the nuclear export of histone deacetylase 5 (HDAC5) increasing histone acetylation, which appears to activate parts of the pro-regenerative transcription program (Cho et al., 2013). However, it is uncertain if ATF3 fits into this signaling cascade. Peripheral axonal injury induces elevation of Tet3, a DNA demethylase, and 5-hydroxymethylcytosine (5hmC) dioxygenase in adult DRG neurons. Also, DNA demethylation of the ATF3 gene locus regulates ATF3 expression (Weng et al., 2017), but whether this is the only or the major determinant of the injury-induced expression is unclear.

Because ATF3 is such a crucial regulator of sensory and motor neuron regeneration, one strategy for developing effective therapies for peripheral nerve injury may be to identify compounds that enhance its expression. To explore this, we generated an *in vitro hATF3pro* luciferase reporter system and made a *mAtf3-pro*/RmGFP reporter mouse to screen for compounds that increase ATF3 expression in primary sensory neurons. The discovery of topoisomerase inhibitors as ATF3 inducers from this screen led us to explore if DNA breaks occur after peripheral nerve injury.

RESULTS

ATF3 regulator screen

To identify small molecules that induce ATF3 expression and thereby potentially enhance axon regeneration, we designed an *in vitro* luciferase reporter system driven by the human *ATF3* promoter (~35 kb) expressed in a mouse neuroblastoma cell line. We screened this *hATF3pro*/GLuc reporter system with a small focused annotated drug library (596 compounds, mainly enzyme inhibitors; Table S1) as a primary unbiased screen, with DMSO as a negative control. The *hATF3pro*/GLuc reporter cell line was seeded on 384-well plates and treated with compounds at 0.1, 1, or 10 μM for 24 h (Figure 1A). Thirtyeight

compounds increased luciferase activity higher than 1.7-fold (Figure 1B), and they included HDAC, DNMT, and topoisomerase inhibitors (Figure 1C; Table S2). In a secondary screen to confirm potential hits, the *hATF3pro*/GLuc reporter cells were treated with each of the 38 hits at a range of concentrations (0.5 nM to 10 μM), and we assessed both cellular toxicity and luciferase activity (Figure 1A). Twenty of the ATF3 activators, including Chaetocin (a histone lysine methyltransferase inhibitor) (Figure S1A), trichostatin A (TSA; an HDAC inhibitor) (Figure S1B), and the DNA topoisomerase I inhibitor camptothecin (CPT; Figure S1C) are selected for the tertiary screen in primary DRG neurons. The dose-dependent induction of luciferase activity by CPT in the reporter line after a 24-h exposure is shown in Figure 1D.

To examine if the action of the 20 non-toxic ATF3 inducers identified with the hATF3pro/GLuc reporter line translated to activity on primary sensory neurons, we applied these inducers to freshly dissociated adult mouse DRG neuron cultures in a tertiary screen (Figure 1A). Cultured primary DRG neurons from naive mice were seeded on 96-well plates and treated with different concentrations (1 nM to 10 μM) of the hits for 24 h. Of these inducers, CPT and TSA increased neurite outgrowth in primary DRG neurons (Figure 1E). TSA has been reported previously to increase neurite growth in cerebellar granule neurons by induction of histone H3K9/14 hyperacetylation, which enhances GAP43 expression (Gaub et al., 2010; Tedeschi et al., 2009), but it has no effect on axon regeneration in an optic nerve crush model (Gaub et al., 2011). We found that CPT increased ATF3 expression in DRG neurons in a robust dose-dependent way (Figure 1F). Both the ATF3 induction and neurite-promoting actions of CPT were more potent (50 nM) in primary sensory neurons than in the reporter line. We therefore decided to focus on this compound to evaluate its action as an ATF3 inducer on axonal growth in sensory neurons *in vitro* and *in vivo*.

CPT action on primary DRG neurons *in vitro*

To further evaluate CPT's ATF3-inducing action in primary DRG neurons, we generated a *mAtf3pro*/RmGFP reporter mouse for which RmGFP (Renilla muelleri GFP) expression is driven by the full *mAtf3* (35 kb) promoter (Figure 2A). RmGFP expression was detected at high levels in L3 and L4 DRG neurons ipsilateral but not contralateral to a sciatic nerve injury to the reporter mouse (Figures 2B and 2C). The number of GFP-expressing DRG neurons increased with increasing days post-injury (Figures S2A and S2B). All GFP-positive DRG neurons were immunoreactive for ATF3; however, only ~30% of ATF3 immunoreactive DRG neurons displayed GFP expression at 48-h post-crush. The *mAtf3pro/*RmGFP-positive neurons co-labeled for NF200 and had a large diameter (1,000–3,200 μm^2), whereas injured ($ATF3^+$) small-diameter DRG neurons ($TRPV1^+$ or $IB4^+$) were not GFP positive (Figures S2C and S2D). This finding indicates that the regulation of ATF3 induction for small and large sensory neurons is different and this particular reporter mouse does not capture ATF3 induction in small sensory neurons. RmGFP was robustly expressed in motor neurons in the sciatic motor pool in the ipsilateral ventral horn of the spinal cord. Two days after injury, >90% of ATF3 immunoreactive motor neurons expressed GFP (Figure S2E). When cultured primary DRG neurons from *mAtf3pro*/RmGFP reporter mice were seeded on 96-well plates and treated with different doses of CPT for 24 h, both GFP intensity and neurite extent increased in parallel with increasing doses of CPT (Figure 2D).

To test if the effect of CPT on neurite outgrowth was due to ATF3 induction, CPT was administered to DRG neurons following knockout (KO) of ATF3 by using an inducible *Brn3a::Atf3* KO mouse. The normal increase in neurite outgrowth produced by a preconditioning nerve injury in wild-type (WT)/littermate DRG neurons was abolished in *Brn3a::Atf3* KO DRG neurons, after tamoxifen administration (Figure 2E), and the growth-promoting effects of CPT were also abolished (Figures 2F and 2G). We conclude that the growth-promoting actions of both a preconditioning nerve lesion and CPT treatment are dependent on the induction of ATF3.

Regeneration of sciatic nerve after CPT treatment

CPT administration soon after nerve injury may contribute, through the increased expression of ATF3 and its regulation of RAGs (Renthal et al., 2020), to enhanced axonal regeneration. To test this hypothesis, a sciatic nerve crush was performed in *mAtf3pro*/RmGFP reporter mice (day 0) and the mice administered 2 mg/kg CPT (or vehicle) by intraperitoneal (i.p.) injection 30 min after the crush, followed by consecutive daily injections of CPT or vehicle for 5 days. The injured sciatic nerve was then dissected for quantification of axon regeneration.

A significantly greater extent and number of axons regenerated in the CPT group relative to controls, as observed by SCG10/Stathmin 2 immunostaining (Figures 3A and S3A) with a higher density of SCG10-positive fibers 1 mm distal to the injury site in the CPT- versus vehicle-treated group (Figure 3B) 5 days after injury. In the CPT-treated group, SCG10-positive axons were also present at a significantly higher number (>2-fold) up to 2.5 mm from the crush site, with a trend continuing beyond that level (Figure 3C). The average length of the longest $SCG10^+$ fibers was 6, 136 ± 501 μm in the CPT-injected group compared with 3,796 ± 611 μm in the vehicle-injected group (61.6% increase; $p = 0.025$) (Figure 3D). A higher density of *Atf3*RmGFP-positive axons were also present in the CPT-injected group (Figures S3B–S3D). These data show that hits from a screen for ATF3 inducers can translate into pro-regenerative activity *in vivo*.

Functional recovery from sciatic nerve injury after CPT treatment

A sciatic nerve crush was performed in WT C57/BL6 mice and the mice treated with 2 mg/kg i.p. CPT 30 min after the crush injury, followed by consecutive daily injections for 5 days. Sensory reinnervation of the skin by the injured sensory neurons was measured by the pinprick test applied to the lateral edge of the paw and by functional motor recovery of distal plantar muscles by the toe spreading test (Painter et al., 2014) and sciatic function index measured on a DigiGate system. CPT accelerated both sensory and motor recovery. Significant improvements for both modalities were found 9–10 days after crush, between CPT- and vehicle-injected groups, and these improvements persisted for 5 days in the sensory paradigm and 9 days in the motor (Figures 3E and 3G). In addition, the kinetics of functional recovery indicated an earlier initiation of successful reinnervation (Figures 3F and 3H). At day 15 after the crush injury, the sciatic functional index (SFI) was significantly higher in the CPT-treated group than the vehicle group (Figures 3I and 3J).

CPT elevates ATF3 expression in DRG neurons early after sciatic nerve injury

To explore the transcriptional effects of CPT in DRG neurons, we harvested DRGs (L3–L5) from mice treated with CPT at different times after sciatic nerve injury. We performed a qRT-PCR analysis, which showed that expression of the ATF3 transcript was induced in the DRG soon after sciatic nerve injury and that CPT treatment substantially enhanced this expression at 24 h (Figure 4A). Then, using RNA sequencing (RNA)-seq analysis, we found that multiple RAGs (*Atf3, Gal, Gpr151*, and *Sprr1a*) were induced more after CPT treatment than vehicle-treated mice DRG at 18 and 24 h post-sciatic nerve injury (Figures 4B and 4C). However, expression of ATF3 dropped to levels observed in the vehicle-treated group at 36 h after injury, which is the same as that for other RAGs (Figure S4A). These two datasets indicate that CPT amplifies ATF3 expression but only in the period immediately after nerve injury (18–24 h) (Figures 4A–4C, S4A, and S4B).

Given the substantial increase in nerve regeneration following CPT treatment, we hypothesized that CPT may exert its effects by broadly activating the injury-induced RAG network (Chandran et al., 2016; Renthal et al., 2020). A total of 83 of the 147 transcripts upregulated in DRGs 18 h after CPT injection compared to vehicle were also upregulated after injury, relative to naive DRGs ($Injury^{VEH}$ versus $Naive^{VEH}$, respectively), which is a significant enrichment ($p = 1.33 \times 10^{-24}$, hypergeometric test) (Figure 4D). Similarly, 350 of the 500 genes showing greater downregulation in injured DRGs 18 h after CPT injection were enriched for genes downregulated by nerve injury ($Injury^{VEH}$ versus $Naive^{VEH}$) (hyperGenometric Test, 1.56×10^{-116}). The significance of downregulated genes for nerve regeneration and whether enhancement of this downregulation contributes to the regeneration-promoting effects of CPT remain to be explored. A comparison of the CPT responsive genes to a previously defined regeneration network (Chandran et al., 2016) showed that 14 out of 147 upregulated genes in injured DRGs after CPT-induced stimulation are shared with a regeneration gene set module after nerve injury, which was defined in the earlier study ($p = 4.23 \times 10^{-7}$, hypergeometric test) (Figure S4C). However, 24 h after CPT injection, only 5 out of 23 upregulated genes intersected with the non-treated injured gene set and none with the predefined regeneration gene set (Figures S4E and S4F). This finding indicates that CPT treatment causes an enhanced expression of RAGs early after injury, but the effect is short lived.

Network and pathway analyses further support the pro-regenerative effects of CPT. Gene Ontology analysis of the genes up-regulated in CPT-treated injured DRGs at 18 h revealed a prominent induction of genes involved in cytoskeleton rearrangement, development, and neurogenesis, as well as axon guidance and neuronal differentiation genes (Figures 4E and S4D). This finding implies that the action of CPT is targeted specifically at the regenerative component of the injury-induced transcriptional changes and not those that may contribute to neuropathic pain and reinforces earlier findings that ATF3 expression in sensory neurons immediately after axonal injury initiates the regenerative response to injury.

Sciatic nerve injury induces DNA breaks at the ATF3 gene locus in DRG neurons

Our discovery that ATF3 expression is increased by a topoisomerase inhibitor, together with the involvement of topoisomerases in DNA repair (Sakasai and Iwabuchi, 2016), points to a

possible contribution of DNA breaks in the regulation of ATF3 after nerve injury. Previous work has demonstrated a clear link between DNA damage and robust gene expression. DNA double-strand breaks (DSBs) occur near transcription start sites (TSSs) of highly transcribed genes involved in general cellular processes in various cell types (Schwer et al., 2016), and recurrent DNA breaks clusters have been identified in long, transcribed, and late-replicating genes in neural stem/progenitor cells (Wei et al., 2016). Furthermore, neuronal activity leads to the formation of DNA breaks in a subset of highly induced early-response genes in cortical neurons, and this contributes to their activity-dependent regulation (Madabhushi et al., 2015).

We therefore sought to explore whether DNA breaks are triggered by peripheral nerve injury and if this may lead to ATF3 expression in DRG neurons. DNA breaks produce several well-characterized molecular responses; the gamma-H2AX (γ-H2AX) histone variant becomes phosphorylated on chromatin minutes after formation of DNA breaks (Han et al., 2006); and expression of 53BP1, which is involved in DNA repair signaling, becomes localized to the break site, serving as a marker of DNA breaks (Lassmann et al., 2010). We found that numerous γ-H2AX and p53BP1 foci appear in the nucleus of primary DRG neurons (Figure 5A) 30 min after exposure to sufficient irradiation (IR) to produce genotoxicity and DNA breaks (Casafont et al., 2011). Similar DNA break foci (as detected by 53BP1 and γ-H2AX overlapping puncta), albeit fewer per neuron, were also found in the nuclei of DRG neurons as early as 10 min after a sciatic nerve crush injury (Figure 5A). Although the 53BP1 staining appears fuzzy in the nucleus, it localizes to foci in injured DRG neurons, which is the same as seen in other cell types (Harrigan et al., 2011; Lou et al., 2020; Shanbhag et al., 2019). The peak percentage of neurons with DSD foci occurred 30 min after the nerve injury, with a second but smaller increase at 24 h after the injury (Figure 5B).

To determine whether these DNA breaks were localized to the ATF3 gene locus, we performed chromatin immunoprecipitation (ChIP) and quantitative PCR (qPCR) for 53BP1 on DNA from the DRG of naive mice or mice with sciatic nerve crush. Nerve crush led to an enrichment of 53BP1 binding at the promoter and second exon of the ATF3 gene (Figure 5C). The binding appeared to be localized to the early portion of the ATF3 gene body, as no enrichment was observed at the 3′ UTR of ATF3. There was also no binding in either the c-JUN or the TATA Box binding protein (TBP) gene (Figure S5A). Insufficient DNA was obtained from injured DRG neurons, and thus, we were unable to conduct a genome-wide ChIP sequencing (ChIP)-seq analysis.

CPT enhances DNA breaks at the ATF3 gene locus in the DRG

The fact that ATF3 expression is elevated in injured DRG neurons (Figure 4A) and DNA breaks are enriched at the ATF3 gene locus in these neurons immediately after sciatic nerve injury (Figure 5C) raises the question whether DNA breaks induce ATF3 expression after sciatic nerve crush. Certainly, the finding that ATF3 transcript expression is enhanced by CPT, a DNA break-inducer (Figure 4A), supports this possibility. To determine directly if CPT leads to increased DNA breaks in injured DRG neurons, CPT was administered 30 min before a sciatic nerve injury; injured DRGs were collected 5, 30, and 120 min after the nerve crush, and DNA break foci were measured in DRG neuron nuclei (Figure 6A).

DNA breaks in injured DRG neurons were enhanced by CPT at 5–30 min post-nerve injury (Figure 6B). To determine whether this enhancement was localized to the ATF3 locus, we ran ChIP-qPCR for 53BP1 and γ-H2AX on DNA from injured and non-injured DRGs after vehicle or CPT treatment. CPT treatment increased 53BP1 or γ-H2AX binding at both the promoter and exon 2 of the ATF3 gene in injured and non-injured DRG neurons significantly greater than that in vehicle-treated mice (Figures 6C, 6D, and S5B) but had no effect on the c-Jun or TBP genes (Figure S5C). DNA breaks are induced then, rapidly after sciatic nerve injury at the *mAtf3* gene locus, and CPT both further elevates this and ATF3 expression. This result suggests that induction of DNA breaks may contribute to the regulation of this key regeneration-promoting transcription factor after axonal injury, and this would explain why enhancing the DNA breaks induction pharmacologically increases regeneration.

DISCUSSION

Injured axons of sensory and motor neurons regenerate in the PNS, whereas those in the CNS cannot. A major contributor to this difference is that after axonal injury PNS neurons undergo a major change in their gene expression that shifts them from a growth-quiescent into an actively growing or regenerative state. This change occurs through distinct temporal phases of gene induction. Multiple genes coding for transcription factors respond early (within a few hours) after nerve injury, including AP1, JUN, CREB, STAT3, NF-κB, SOX11, and ATF3 (Jing et al., 2012; Patodia and Raivich, 2012; Renthal et al., 2020; Seijffers et al., 2007; Van der Zee et al., 1989). These early-response genes then act in a coordinated manner to master regulate later expression of effector-regeneration-promoting genes (Chandran et al., 2016; Renthal et al., 2020). Although this response is sufficient to promote successful regeneration in rodent models (Ma et al., 2011), in humans, long distances hamper successful functional reinnervation of peripheral targets after proximal injuries. It would therefore be beneficial if regeneration could be enhanced or accelerated. One way to do this experimentally is to prime injured neurons for growth by a preconditioning nerve injury. The initial insult of the preconditioning injury induces the RAG network, resulting in an even greater further induction of these genes and faster growth of axons in response to a subsequent second nerve injury (Nix and Bastiani, 2012; van Kesteren et al., 2011; Yang et al., 2021).

Preconditioning injury cannot be used clinically, of course. Although, can one pharmacologically mimic the amplifying effects of a preconditioning lesion on RAGs? Our approach to address this was to search for compounds that enhance induction of arguably the most important regeneration master regulator, the transcription factor ATF3. ATF3 is absent or expressed at very low levels in naive non-injured DRG neurons but is quickly (within a few hours) induced up to 30-fold after axotomy. This change occurs only in neurons that can regrow (Tsujino et al., 2000). Constitutive ATF3 expression in non-injured DRG neurons recapitulates many of the effects of a preconditioning nerve injury, increasing the expression of RAGs and enhancing peripheral nerve regeneration (Seijffers et al., 2007). The reverse is true in ATF3 KO mice, in which induction of RAGs is reduced and axon regeneration decreased in injured motor neurons (Gey et al., 2016; Renthal et al., 2020). Here, we find

that selective KO of ATF3 in adult DRG neurons from *Brn3a::Atf3KO* mice eliminates the preconditioning effect.

Our ATF3 reporter screen detected several classes of ATF3-inducing compounds, with HDAC, DNA methyltransferase (DNMT), and topoisomerase inhibitors being the most represented targets. Because epigenetic modifiers, including HDAC and DNMT inhibitors, have already been reported to increase axonal regeneration, we decided to investigate here if there is a link between topoisomerase inhibition, ATF3 expression, and axonal regeneration, which is something not described before.

There are seven mammalian topoisomerases, including four type I (TOP I) and three type II (TOP II) (Champoux, 2001). TOP I can be further divided into type IA and IB based on the side of the DNA break (Wang, 2002). The key function of TOP I is to relax DNA supercoiling. Therefore, these enzymes tend to be concentrated in supercoiled chromatin regions, particularly in association with transcription or replication complexes (Wang, 2002). CPT, a cytotoxic quinoline alkaloid, inhibits TOP1, preventing the re-ligation of nicked DNA that leads to an accumulation of a transient intermediate of normal topoisomerase activity, termed TOP1 cleavage complexes (TOP1ccs). The accumulation of TOP1ccs and associated nicks eventually lead to the generation of DNA DSBs at sites of TOP1 activity (Cristini et al., 2019). Depletion of Top1 in excitatory neurons causes genomic instability and DNA breaks (Fragola et al., 2020).

Having found CPT, a well-described promoter of DNA breaks, to be an ATF3 inducer in injured primary sensory neurons and knowing that DNA breaks occur at highly induced genes in many systems (Bunch et al., 2015; Cristini et al., 2019; Ju et al., 2006; Madabhushi et al., 2015), we explored whether nerve injury induces DNA double-strand breaks (DSBs) and if they occur at the ATF3 locus. DNA breaks do indeed appear in DRG neurons within minutes after a sciatic nerve injury. This is much quicker than the rapid induction of ATF3 (which takes several hours), one of the earliest injury-regulated genes. Furthermore, CPT enhances the numbers of DNA breaks at the ATF3 gene locus in injured DRG neurons, within 30 mins. We conclude that nerve injury generates DNA breaks at the ATF3 locus and that they may be involved in the induction of ATF3 transcription. The enhanced axonal regeneration induced by CPT is likely to be contributed to by the production of more DNA breaks at the ATF3 gene locus and increased ATF3 transcription because forced ATF3 expression is sufficient to increase regeneration (Seijffers et al., 2007). DNA DSBs also occur in CNS neurons, but increasing evidence indicates that DNA damage and genomic instability in these neurons drive human CNS neurodegenerative disorders related to altered gene transcription (Cristini et al., 2020; Sordet et al., 2009). Why DNA breaks in sensory neurons are not associated with cell death but are in central neurons needs to be explored and whether or not this relates to the failure of CNS neurons to regenerate after axonal injury.

Although genome integrity is a fundamental element of cell survival, topoisomerase-induced DNA breaks do control transcription in specific circumstances. How DNA breaks develop at a particular gene locus to produce rapid transcription is an active area of study. Deng et al. (2015) showed that a TOP2A inhibitor triggers DNA breaks in cancer cells, followed

by activation of the DNA damage response. This DNA damage response was shown by enhanced γ-H2AX/53BP1 foci accumulation and triggered an ATF3 induction in ATM (ataxia telangiectasia mutated)-dependent manner (Deng et al., 2015). Torsional strain, in addition to being a by-product of transcription and DNA replication, can hold promoters in an inactive but poised transcriptional state (Madabhushi et al., 2015). Resolution of the torsional strain by topoisomerase-induced DNA breaks allows RNA polymerase II (RNA Pol II) bound to the promoter to enter the gene body and start transcription. This model is consistent with the rapid but transient effects of CPT on ATF3 induction (Figure 4A). Another theory is that DNA breaks increase the rate of transcription through the gene body. Transcription elongation usually requires changes in the local supercoiled state of DNA to form positive supercoils ahead and negative supercoils behind the transcription machinery (Liu and Wang, 1987). DNA topoisomerases solve such DNA topological issues during DNA transcription (Wang, 2002) by introducing transient DNA breaks, using a transesterification mechanism that is reversible and minimizes risks to genome stability (Wang, 2002). Finally, DNA breaks can have topology-independent mechanisms for promoting transcription, including RNA Pol II phosphorylation by DNA-break-induced signaling (Bunch et al., 2015). These mechanisms are not mutually exclusive, and all may lead to the expression of ATF3 following nerve injury and its facilitation on exposure to a topoisomerase inhibitor.

How does nerve injury produce DNA breaks? Krishnan et al. (2017) showed that axonal injury triggers BRCA-1-dependent DNA breaks in neurons and supports an enabling transcriptional program of injured DRGs. Another possibility is the calcium wave generated at the injury site that moves retrogradely along axons to the cell body (Doron-Mandel et al., 2015). Axonal transection triggers an influx of calcium to the millimolar range near the tip of the cut axon and in the micromolar range in axons proximal to the cut end (Ziv and Spira, 1995). Intracellular calcium activates many calcium-sensitive enzymes, including the proteolytic enzyme calpain. Activated calpain-2 enters the nucleus where it truncates nuclear topoisomerase (Kanungo et al., 2009) that can interact with nucleolin to form cleavable complexes at genomic DNA (Chou et al., 2011), in a manner similar to topoisomerase inhibitors. The elevation of calcium and the subsequent calpain activation it produces in the cell body of DRG neurons occurs within an hour after nerve injury, a timescale comparable to the induction of DNA breaks we observed after nerve injury (Figure 7; Glass et al., 2002). The induction of topoisomerase activity in injured DRG neurons by calcium might explain our findings that CPT administration to non-injured mice was not sufficient to induce ATF3 expression. A similar cascade may occur with activity-dependent gene expression in cortical neurons. Neurons initiate transcriptional programs for immediate early genes (IEGs) in response to activity (Ebert and Greenberg, 2013; Murai et al., 2020). Activity-triggered DNA breaks in IEGs drive the expression of Fos, FosB, Npas4, and Egr1 in immature cortical neurons (Madabhushi et al., 2015), and it is possible, therefore, that activity, and the calcium influx it produces through voltage-gated calcium channels, contributes to injury-induced DNA breaks. However, it is still unclear if the neuronal activity initiated by axotomy (injury discharge) (Sapunar et al., 2005) is sufficient to drive the expression of RAGs in DRG neurons; certainly, other conditions that increase activity in

DRG neurons such as peripheral inflammation do not induce RAG expression, and this suggests that the calcium wave resulting from axonal injury may be required.

The discovery, through a screen for ATF3 inducers, that the TOP I inhibitor CPT amplifies ATF3 expression in injured sensory neurons and that this enhances neurite growth and regeneration opens the possibility that topoisomerase inhibitors may be, at least at the time of or soon after injury, potential therapeutics for accelerating nerve regeneration, acting as transcription enhancers. Several CPT analogs are FDA approved for cancer treatment, and whether or not these drugs can be safety repurposed for early enhancement of regeneration after nerve injury needs to be examined. The discovery of the pro-regenerative action of a TOP1 inhibitor led us to the novel observation that nerve injury induces DNA breaks at the ATF3 locus, providing new insights into how the induction of the complex gene program required for axon regrowth may be initiated.

STAR★METHODS

RESOURCE AVAILABILITY

Lead contact—Further information and requests for resources and reagents should be directed to and will be fulfilled by lead contact, Clifford Woolf (Clifford.woolf@childrens.harvard.edu).

Materials availability—All reagents generated in this study are available from the lead contact with a completed Materials Transfer Agreement.

Data and code availability

- All data reported in this paper will be available from the lead contact upon reasonable request.
- Scripts used in the RNA-seq analyses are available at https://github.com/icnn/RNAseq-PIPELINE. Raw and processed data were deposited within the Gene Expression Omnibus (GEO) repository (https://www.ncbi.nlm.nih.gov/geo) with an accession number (GSE113672) and is publicly available as of the date of publication.
- Any additional information required to reanalyze the data reported in this paper is available from the lead contact upon request.

EXPERIMENTAL MODEL AND SUBJECT DETAILS

hATF3pro/GLuc stable cell line—A fosmid bearing the human *ATF3* promoter, tagged with a Gaussia Luciferase/pA reporter immediately upstream of the 5′ end of *hATF3* coding sequence, was obtained from Spectragenetics Biotech. A mouse neuroblastoma cell line (B104) was transfected with the *hATF3pro*/GLuc Fosmid by Lipofectamine 2000 through a standard transfection protocol. Forty-eight hours after transfection, cells were treated with 1 mg/ml neomycin for another 48 hours for single stable clone selection.

Mice—8-12 week-old C57BL/6J mice (strain #000664; RRID:IMSR_JAX:000664) were obtained from Jackson Laboratory (Bar Harbor). Animals were housed and handled in accordance with protocols approved by the institutional animal care and use committee (IACUC) of Boston Children's Hospital. Male mice were used in all experiments. All mice were aged matched.

mAtf3pro/RmGFP reporter mice—A fosmid-containing the mouse *Atf3* promoter, tagged with a Renilla Mulleri GFP (RmGFP) reporter at the 5′ end of the *mAtf3* coding sequencing, was obtained from Spectragenetics Biotech. The *mAtf3pro*/RmGFP fosmid was linearized by lambda-terminase and purified by UltraPure Phenol:Chloroform:Isoamyl Alcohol (25:24:1, v/v) and precipitated by sodium acetate. The purified pellet was washed 3 times in 75% ethanol, and then dissolved in microinjection buffer (Tris-EDTA, pH = 7.5). Samples were diluted to 1~5 ng/ul for pronuclear microinjection, carried out by the IDDRC Mouse Gene Manipulation Core at Boston Children's Hospital. Male mice were used in all experiments. All mice were aged matched.

Atf3 flox/flox mice—Inserting loxP sites around exon 3 of the mouse *Atf3* gene. *Brn3a-Cre*^{ERT2}::*Atf3 flox/flox* mice were generated by crossing the *Atf3 flox/flox* mice with *Brn3a-Cre*^{ERT2} (JAX strain #032594; RRIDIMSR_JAX:032594) mice. Littermate controls were used for experiments. All mice were aged matched.

METHOD DETAILS

Sciatic nerve crush—All surgeries were performed aseptically under 2.5% isoflurane. The sciatic nerve was exposed at mid-thigh level on the left side of the mice and crushed with smooth forceps for 30 s and the wound closed in two layers.

Tamoxifen treatment—Tamoxifen (Sigma) was dissolved in corn oil at 20 mg/mL. Mice were injected intraperitoneally with 75 mg/kg tamoxifen for five consecutive days. All injected mice were observed daily for any abnormalities. Vehicle control is corn oil only.

In vitro* luciferase screening system—hATF3pro*/GLuc stable cell lines were seeded onto a 384-wells plate and screened with small compound libraries for 24 hr. Luciferase substrate was added into the wells 24 hr post-treatment, and luciferase activity detected using the EnVision multi-label luminescence plate reader.

Quantitative real-time PCR and western immunoblotting—Total RNA was extracted from *hATF3pro*/GLuc reporter cell lines or primary DRG neurons using TRIzol (ThermoFisher). cDNA synthesis was performed using Superscript III reverse transcriptase (ThermoFisher) primed with Oligo-dT. Quantitative PCR (Q-PCR) reactions used SYBR Green PCR Master Mix (ThermoFisher) and were run on ABI 7500 Real Time PCR System. Expression of GLUC, *hATF3, mAtf3, c-Jun, Egr-1, Gap43, Sprr1a, Sox1* and *Hsp27* were determined after normalization to the housekeeping gene *GAPDH.* Primers are listed in Table S3. Protein lysates from the *hATF3pro*/GLuc reporter cell line were extracted in presence of a protease cocktail tablet (Roche Diagnostics) and phosphatase inhibitor tablet (Roche Diagnostics) using Cell IP-lysis buffer (ThermoFisher), and cell debris removed

by centrifugation (4°C, 10 min). Protein concentrations were determined using the BCA protein assay kit (ThermoFisher). Equivalent amounts of protein were loaded and separated by 4%–12% gradient SDS-PAGE and subsequently transferred to an Immobilon-P PVDF transfer membrane (EMD Millipore). Blots were blocked in 5% blotting-grade blocker (Bio-rad) in PBS for 20 min at room temperature (RT) and incubated with rabbit polyclonal antibodies against total c-JUN (Cell Signaling, 1:1000), ATF3 (Santa Cruz, 1:500), and Horseradish peroxidase (HRP)-conjugated mouse monoclonal antibody against GAPDH (Cell Signaling, 1:5000) overnight. After washing 3 times with TBST (1% Tween-20), HRP-conjugated secondary antibody (anti-rabbit, ThermoFisher, 1: 20,000), a SuperSignal West Femto Maximum Sensitivity chemiluminescence ECL kit (ThermoFisher), and Amersham Hyperfilm ECL (GE Healthcare Life Sciences) were used for signal detection. Image signals were analyzed and quantified using ImageJ software (NIH).

Neurite outgrowth analysis—Primary DRG sensory neurons were isolated, purified and plated on 96-well Poly-D-Lysine (PDL) coated plates with or without laminin. Compounds were added to the well and DRG neurons fixed after 3 days and stained using a mouse monoclonal antibody against bIII-tubulin (TUJ1), a rabbit polyclonal antibody against ATF3 and Hoechst for nuclear staining. Neurite outgrowth was analyzed with an ArrayScan High Content Screening System (Cellomics). Data including neuron counts, neuronal cell body area, neurite total length, neurite maximum length and GFP intensity were collected with a neuron selecting algorithm. Pictures were acquired with a 10x objective using the ArrayScan high-resolution camera mode and analyzed based on the “Neuronal profiling” bioapplication.

Immunohistochemistry—Dorsal root ganglia (DRG) and spinal cords were harvested from injured *mAtf3pro*/RmGFP reporter mice perfused with ice-cold PBS followed by cold 4% paraformaldehyde (PFA). In addition, sciatic nerves were harvested distal to the crush in treated *mAtf3pro*/RmGFP reporter mice perfused with cold 4% PFA. Perfused tissues were post-fixed for 3 hr at 4°C, and cryoprotected with 30% sucrose in PBS overnight. DRG sections (10 μm), spinal cord sections (20 μm) and sciatic nerve sections (60 μm) collected, blocked and permeabilized with 1% Triton X-100 in blocking buffer (Roche Diagnostics) for 1 hr at RT. Sections were incubated with rabbit polyclonal antibody against ATF3 (Santa Cruz Biotech; sc-188; 1:1000), TRPV1 (Alomone; ACC-030; 1:1000), SCG10 (Novus; NBP1-49461; 1:2000), 53BP1 (Novus; NB100-304; 1:2000), chicken polyclonal antibody against NF200 (Millipore, AB5539; 1:2000), rat polyclonal antibody against Laminin-γ (Millipore; MAB-1914P; 1:1000), DyLignt_594 conjugated Isolectin B4 (VectorLab; DL-1207; 1: 200), or mouse monoclonal antibody against phospho-Histone H2A.X (Ser139)(γ-H2AX; gamma-H2AX) (Millipore; 05-636; 1:400) at 4°C overnight and then incubated with Alexa Fluor 568 goat antibody against rabbit IgG, chicken IgG or rat IgG for 1 hr at RT. Images were acquired using a Nikon Eclipse 80I Microscope.

RmGFP intensity analysis—To quantify GFP intensity in *mAtf3pro*/RmGFP reporter DRGs after compound treatment, DRGs 2-days post-injury were isolated, purified and plated in 384-well clear-bottom assay plates (Greiner) coated with poly-D-lysine and laminin at a cell density of 2,000/well. Twenty-four hours after plating, Relative

Fluorescence Units (RFU) was measured and analyzed using a Functional Drug Screening System (FDSS7000, Hamamatsu).

Quantification of axon regeneration—After a sciatic nerve crush, *mAtf3pro*/RmGFP reporter mice were treated with 2 mg/kg CPT for 5 days. Sciatic nerves were then dissected distal to the crush site and fixed with 4% PFA. Regenerating axons were visualized by staining with primary antibody against SCG10 (1:1000). Axons were counted at specified distances from the injury site using a semi-automated fiber quantification method using ImageJ software (NIH).

Assessment of functional recovery—A pinprick assay was performed to assess sensory recovery after sciatic nerve crush. Briefly, mice were habituated on wire mesh cages for at least 30 min and then tested for nociceptive withdrawal responses on the hind paw using a small insect needle. The toe-spreading assay was performed to assess motor recovery. Mice were gently covered with a piece of cloth and lifted by the tail, uncovering the hind paws for clear observation, and the number of toes and extent of toe spreading was measured for the injured side and compared to the uninjured paw. Motor recovery in sciatic nerve injured mice was also recorded using DigiGait apparatus (Mouse Specific), and the sciatic nerve functional index (SFI) calculated (Sakuma et al., 2016). Experiments were conducted fully blinded to drug treatment and surgery.

RNA-seq library preparation and sequencing—DRG tissue samples were harvested from naive and injured mice after five daily injections with Camptothecin or vehicle. Total RNAs were extracted from these DRG tissue samples using TRIzol (ThermoFisher), and then purified using total RNA mini kit (QIAGEN). Quality control assessment of these purified RNA samples was conducted using Bioanalyzer (Agilent) and the RNA integrity numbers (RIN) of all RNA samples submitted for sequencing were > 7.

RNA-sequencing was carried out using the NuGEN Ovation RNA Ultra Low Input kit and TruSeq Nano. Libraries were indexed and sequenced by HiSeq2500/HiSeq4000 with 69-bp paired end reads.

Quality control (QC) was performed on base qualities and nucleotide composition of sequences, to identify problems in library preparation or sequencing. Reads were trimmed and filtered if necessary after the QC before input to the alignment stage. Reads were aligned to the latest Mouse mm10 reference genome (GRCm38.75) using the STAR spliced read aligner (ver 2.4.0). Average input read counts were 63.7M per sample and average percentage of uniquely aligned reads were 76.5% Total counts of read-fragments aligned to known gene regions within the mouse (mm10) refSeq (refFlat ver 07.24.14) reference annotation are used as the basis for quantification of gene expression. Fragment counts were derived using HTSeq program (ver 0.6.0). Batch effect was removed using Bioconductor package ComBat and RUV (removal of unwanted variation). Differentially expressed genes were identified using the Bioconductor package edgeR (FDR = 0.1). Scripts used in the RNA sequencing analyses are available at http://github.com/icnn/RNAseq-PIPELINE. Raw and processed data were deposited within the Gene Expression Omnibus (GEO) repository (https://www.ncbi.nlm.nih.gov/geo) with an accession number (GSE113672).

Image analysis and quantification of DNA double-strand breaks (DSBs)— Digital Z stack images (40X and 20X objective lens) were obtained with sequential acquisition setting by confocal microscopy (LSM laser-scanning confocal microscopy; Zeiss). We applied ImageJ software to analyze the images to adjust brightness and contrast for the quantitative analysis of DNA DSB foci (double-positive signal of γ-H2AX and 53BP1; yellow dots). The co-localization signal of γ-H2AX (green signal) and 53BP1 (red signal) staining was based on the yellow signal (dots) indicated in the images. The definition of DNA DSB foci (puncta): the yellow dot should be larger than 0.1 μm^3 volume or at least 60 mean gray values in an 8-bit scale. The position of the nucleus was judged by DAPI staining. The average field was calculated from 10 images. First, the DRG neurons were selected based on the DAPI staining and the size of the nucleus from each image. In these DRG neurons, the double-positive signal (yellow dots) of γ-H2AX and 53BP1 channels through manual counting were used to calculate the DNA DSB foci. Then, the proportion of neurons with DNA DSB foci in total DRG neurons per image was calculated

Chromatin immunoprecipitation (ChIP) qPCR—L3,4,5 DRGs from C57/BL6 mice were harvested and flash frozen in liquid nitrogen. 18 frozen DRGs were pooled in each sample for chromatin immunoprecipitation (ChIP). DRGs were thawed in cold TBH buffer (250 mM sucrose, 20 mM Tris (pH 7.4), protease inhibitors) and dissociated using twenty-five strokes of a 7mL dounce homogenizer. Dissociated cells were fixed in TBH containing 1% formaldehyde for 10 minutes. Fixation was quenched with 125mM glycine for 5 minutes and cell pelleted at 3000 g for 5 minutes at 4C. Nuclei were isolated from the cell pellet by incubating in 1mL cell lysis buffer (5 mM HEPES, pH 8, 85 mM KCl, 1 mM EDTA, 0.5% NP-40, protease inhibitors) for 10 minutes at 4C, after which nuclei were sedimented at 3000 g for 5 minutes at 4C. Nuclei were lysed in 150 μL nuclear lysis buffer (50 mM Tris-Cl, pH 8, 10 mM EDTA, 1% SDS, protease inhibitors) for 10 minutes at RT. 850 μL dilution buffer (16.7 mM Tris-Cl, pH 8, 167 mM NaCl, 1.2 mM EDTA, 1% Triton X-100, 0.1% SDS, protease inhibitors) was added to the 150 μL nuclear lysis reaction. The 1mL chromatin was sonicated for 20 minutes (high power, 30 s ON/30 s OFF) in a Diagenode Bioruptor sonicator (Diagenode UCD-200). Sheared chromatin was centrifuged at 13,000 g for 10 minutes. The soluble chromatin phase was transferred to a fresh tube and insoluble material discarded. The soluble chromatin segments were pre-cleared with 20 μL Dynabeads protein A (Invitrogen, 10002D) at 4C for 2 hours. $1/10^{th}$ of the pre-cleared chromatin was reserved as input and the remainder was incubated with 5 μg Anti-53BP1 antibody (Novus, NB100-304) at 4C overnight, followed by adding 40 μL Dynabeads protein A for another 4 hours. The enriched segments were washed sequentially with buffer LS (0.1% SDS, 1% Triton X-100, 2 mM EDTA, 150 mM NaCl, 20 mM Tris-Cl, pH 8), buffer HS (0.1% SDS, 1% Triton X-100, 2 mM EDTA, 500 mM NaCl, 20 mM Tris-Cl, pH 8), buffer TL (1% NP-40, 1% NaDOC, 1 mM EDTA, SDS, 0.25 M LiCl, 50 mM Tris-Cl, pH 8) and buffer TE (0.1 mM EDTA, 50 mM NaCl, 10 mM Tris-Cl, pH 8) for 5 minutes each. Chromatin was then eluted in 145uL elution buffer (1% SDS, 0.1 M NaHCO3) for 25 minutes at 65C and 800rpm. Crosslinking was reversed with NaCl and EDTA so that the final solution contained 0.2 M NaCl and 0.1 mM EDTA and incubating for 18hr at 65C and 800rpm. The de-crosslinked samples was purified using QIAGEN MinElute PCR purification columns (QIAGEN, 28004) according to the manufacturer's instructions. qPCR

was performed using Sybr Fast Green Mix (Thermo Fischer, 4385610). 53BP1 occupancy at each genomic location was calculated using the percent input method.

QUANTIFICATION AND STATISTICAL ANALYSIS

Statistical analysis was performed using GraphPad PRISM 8 (GraphPad Software, Inc). Statistical analyses, including the number of animals or biological replicates (n) and P values for each experiment, are noted in the figure legends. A hypergeometric test was used to test the significance of the overlap between two gene sets. Unpaired two-tailed t test and two-way ANOVA were used in most experimental analyses. In addition, for multiple comparisons, two-way ANOVA with Bonferroni multiple comparisons test or one-way ANOVA with Fisher's LSD test, Bonferroni's correction with multiple comparisons, or one-way ANOVA with Sidak comparisons test was performed. Data are represented as Mean ± SEM.

Supplementary Material

Refer to Web version on PubMed Central for supplementary material.

ACKNOWLEDGMENTS

We thank Michael. E. Greenberg (HMS) for discussion about this project and express our gratitude to Daniel Tom in the Enhanced Neuroimaging Core of Harvard NeuroDiscovery Center for use of resources and expertise. This work was supported by the New York Stem Cell Foundation (NYSCF) (L.L.R. and C.J.W.), the Harvard Stem Cell Institute (HSCI) (L.L.R. and C.J.W.), the NIH grants R35NS105076 (C.J.W.) and HD090255 (IDDRC Cores), and the Dr. Miriam and Sheldon G Adelson Medical Research Foundation (AMRF) (G.C. and C.J.W.). We thank Kent Nybakken for assisting with the MTS assay on the secondary screen. F.W.A. is an HHMI Investigator. Graphical abstract was designed by Y.-C.C. and created with BioRender.com.

REFERENCES

Bunch H, Lawney BP, Lin YF, Asaithamby A, Murshid A, Wang YE, Chen BP, and Calderwood SK, (2015). Transcriptional elongation requires DNA break-induced signalling. Nat. Commun6, 10191. [PubMed: 26671524]

Campbell G, Hutchins K, Winterbottom J, Grenningloh G, Lieberman AR, and Anderson PN, (2005). Upregulation of activating transcription factor 3 (ATF3) by intrinsic CNS neurons regenerating axons into peripheral nerve grafts. Exp. Neurol192, 340–347. [PubMed: 15755551]

Casafont I, Palanca A, Lafarga V, Berciano MT, and Lafarga M, (2011). Effect of ionizing radiation in sensory ganglion neurons: organization and dynamics of nuclear compartments of DNA damage/repair and their relationship with transcription and cell cycle. Acta Neuropathol. 122, 481–493. [PubMed: 21915754]

Champoux JJ, (2001). DNA topoisomerases: structure, function, and mechanism. Annu. Rev. Biochem70, 369–413. [PubMed: 11395412]

Chan KM, Gordon T, Zochodne DW, and Power HA, (2014). Improving peripheral nerve regeneration: from molecular mechanisms to potential therapeutic targets. Exp. Neurol261, 826–835. [PubMed: 25220611]

Chandran V, Coppola G, Nawabi H, Omura T, Versano R, Huebner EA, Zhang A, Costigan M, Yekkirala A, Barrett L, et al. (2016). A Systems-Level Analysis of the Peripheral Nerve Intrinsic Axonal Growth Program. Neuron 89, 956–970. [PubMed: 26898779]

Cho Y, Sloutsky R, Naegle KM, and Cavalli V, (2013). Injury-induced HDAC5 nuclear export is essential for axon regeneration. Cell155, 894–908. [PubMed: 24209626]

Chou SM, Huang TH, Chen HC, and Li TK, (2011). Calcium-induced cleavage of DNA topoisomerase I involves the cytoplasmic-nuclear shuttling of calpain 2. Cell. Mol. Life Sci68, 2769–2784. [PubMed: 21086148]

Cristini A, Ricci G, Britton S, Salimbeni S, Huang S-N, Marinello J, Calsou P, Pommier Y, Favre G, Capranico G, et al. (2019). Dual Processing of R-Loops and Topoisomerase I Induces Transcription-Dependent DNA Double-Strand Breaks. Cell Rep. 28, 3167–3181.e6. [PubMed: 31533039]

Cristini A, Gromak N, and Sordet O, (2020). Transcription-dependent DNA double-strand breaks and human disease. Mol. Cell. Oncol7, 1691905. [PubMed: 32158914]

Deng S, Yan T, Nikolova T, Fuhrmann D, Nemecek A, Gödtel-Armbrust U, Kaina B, and Wojnowski L, (2015).The catalytic topoisomerase II inhibitor dexrazoxane induces DNA breaks, ATF3 and the DNA damage response in cancer cells. Br. J. Pharmacol172, 2246–2257. [PubMed: 25521189]

Doron-Mandel E, Fainzilber M, and Terenzio M, (2015). Growth control mechanisms in neuronal regeneration. FEBS Lett. 589, 1669–1677. [PubMed: 25937120]

Ebert DH, and Greenberg ME, (2013). Activity-dependent neuronal signalling and autism spectrum disorder. Nature493, 327–337. [PubMed: 23325215]

Fagoe ND, Attwell CL, Kouwenhoven D, Verhaagen J, and Mason MR, (2015). Overexpression of ATF3 or the combination of ATF3, c-Jun, STAT3 and Smad1 promotes regeneration of the central axon branch of sensory neurons but without synergistic effects. Hum. Mol. Genet24, 6788–6800. [PubMed: 26385639]

Fragola G, Mabb AM, Taylor-Blake B, Niehaus JK, Chronister WD, Mao H, Simon JM, Yuan H, Li Z, McConnell MJ, and Zylka MJ, (2020). Deletion of Topoisomerase 1 in excitatory neurons causes genomic instability and early onset neurodegeneration. Nat. Commun11, 1962. [PubMed: 32327659]

Gaub P, Tedeschi A, Puttagunta R, Nguyen T, Schmandke A, and Di Giovanni S, (2010). HDAC inhibition promotes neuronal outgrowth and counteracts growth cone collapse through CBP/p300 and P/CAF-dependent p53 acetylation. Cell Death Differ. 17, 1392–1408. [PubMed: 20094059]

Gaub P, Joshi Y, Wuttke A, Naumann U, Schnichels S, Heiduschka P, and Di Giovanni S, (2011). The histone acetyltransferase p300 promotes intrinsic axonal regeneration. Brain134, 2134–2148. [PubMed: 21705428]

Gey M, Wanner R, Schilling C, Pedro MT, Sinske D, and Knöll B, (2016). Atf3 mutant mice show reduced axon regeneration and impaired regeneration-associated gene induction after peripheral nerve injury. Open Biol. 6, 160091. [PubMed: 27581653]

Glass JD, Culver DG, Levey AI, and Nash NR, (2002). Very early activation of m-calpain in peripheral nerve during Wallerian degeneration. J. Neurol. Sci196, 9–20. [PubMed: 11959150]

Hai T, and Hartman MG, (2001). The molecular biology and nomenclature of the activating transcription factor/cAMP responsive element binding family of transcription factors: activating transcription factor proteins and homeostasis. Gene273, 1–11. [PubMed: 11483355]

Hai T, Wolfgang CD, Marsee DK, Allen AE, and Sivaprasad U, (1999). ATF3 and stress responses. Gene Expr. 7, 321–335. [PubMed: 10440233]

Han J, Hendzel MJ, and Allalunis-Turner J, (2006). Quantitative analysis reveals asynchronous and more than DSB-associated histone H2AX phosphorylation after exposure to ionizing radiation. Radiat. Res765, 283–292.

Harrigan JA, Belotserkovskaya R, Coates J, Dimitrova DS, Polo SE, Bradshaw CR, Fraser P, and Jackson SP, (2011). Replication stress induces 53BP1-containing OPT domains in G1 cells. J. Cell Biol193, 97–108. [PubMed: 21444690]

Huang WL, Robson D, Liu MC, King VR, Averill S, Shortland PJ, and Priestley JV, (2006). Spinal cord compression and dorsal root injury cause up-regulation of activating transcription factor-3 in large-diameter dorsal root ganglion neurons. Eur. J. Neurosci23, 273–278. [PubMed: 16420436]

Huang L, Quan X, Liu Z, Ma T, Wu Y, Ge J, Zhu S, Yang Y, Liu L, Sun Z, et al. (2015). c-Jun gene-modified Schwann cells: upregulating multiple neurotrophic factors and promoting neurite outgrowth. Tissue Eng. Part A 21, 1409–1421. [PubMed: 25588149]

Jankowski MP, Cornuet PK, Mcllwrath S, Koerber HR, and Albers KM, (2006). SRY-box containing gene 11 (Sox11) transcription factor is required for neuron survival and neurite growth. Neuroscience143, 501–514. [PubMed: 17055661]

Jing X, Wang T, Huang S, Glorioso JC, and Albers KM, (2012). The transcription factor Sox11 promotes nerve regeneration through activation of the regeneration-associated gene Sprr1a. Exp. Neurol233, 221–232. [PubMed: 22024412]

Ju BG, Lunyak VV, Perissi V, Garcia-Bassets I, Rose DW, Glass CK, and Rosenfeld MG, (2006). A topoisomerase IIbeta-mediated dsDNA break required for regulated transcription. Science312, 1798–1802. [PubMed: 16794079]

Kanungo J, Zheng YL, Amin ND, and Pant HC, (2009). Targeting Cdk5 activity in neuronal degeneration and regeneration. Cell. Mol. Neurobiol29, 1073–1080. [PubMed: 19455415]

Kool J, Hamdi M, Cornelissen-Steijger P, van der Eb AJ, Terleth C, and van Dam H, (2003). Induction of ATF3 by ionizing radiation is mediated via a signaling pathway that includes ATM, Nibrin1, stress-induced MAPkinases and ATF-2. Oncogene22, 4235–4242. [PubMed: 12833146]

Krishnan A, Purdy K, Chandrasekhar A, Martinez J, Cheng C, and Zochodne DW, (2017). A BRCA1-Dependent DNA Damage Response in the Regenerating Adult Peripheral Nerve Milieu. Mol. Neurobiol55, 4051–4067. [PubMed: 28585187]

Lassmann M, Hänscheid H, Gassen D, Biko J, Meineke V, Reiners C, and Scherthan H, (2010). In vivo formation of gamma-H2AX and 53BP1 DNA repair foci in blood cells after radioiodine therapy of differentiated thyroid cancer. J. Nucl. Med51, 1318–1325. [PubMed: 20660387]

Lee N, Neitzel KL, Devlin BK, and MacLennan AJ, (2004). STAT3 phosphorylation in injured axons before sensory and motor neuron nuclei: potential role for STAT3 as a retrograde signaling transcription factor. J. Comp. Neurol474, 535–545. [PubMed: 15174071]

Li S, Xue C, Yuan Y, Zhang R, Wang Y, Wang Y, Yu B, Liu J, Ding F, Yang Y, and Gu X, (2015). The transcriptional landscape of dorsal root ganglia after sciatic nerve transection. Sci. Rep5, 16888. [PubMed: 26576491]

Lindå H, Sköld MK, and Ochsmann T, (2011). Activating transcription factor 3, a useful marker for regenerative response after nerve root injury. Front. Neurol2, 30. [PubMed: 21629765]

Liu LF, and Wang JC, (1987). Supercoiling of the DNA template during transcription. Proc. Natl. Acad. Sci. USA84, 7024–7027. [PubMed: 2823250]

Lou J, Priest DG, Solano A, Kerjouan A, and Hinde E, (2020). Spatiotemporal dynamics of 53BP1 dimer recruitment to a DNA double strand break. Nat. Commun11, 5776. [PubMed: 33188174]

Ma CH, Omura T, Cobos EJ, Latrémolière A, Ghasemlou N, Brenner GJ, van Veen E, Barrett L, Sawada T, Gao F, et al. (2011). Accelerating axonal growth promotes motor recovery after peripheral nerve injury in mice. J. Clin. Invest 121, 4332–4347. [PubMed: 21965333]

Madabhushi R, Gao F, Pfenning AR, Pan L, Yamakawa S, Seo J, Rueda R, Phan TX, Yamakawa H, Pao PC, et al. (2015). Activity-Induced DNA Breaks Govern the Expression of Neuronal Early-Response Genes. Cell 161, 1592–1605. [PubMed: 26052046]

Mar FM, Bonni A, and Sousa MM, (2014). Cell intrinsic control of axon regeneration. EMBO Rep. 15, 254–263. [PubMed: 24531721]

Moore DL, Blackmore MG, Hu Y, Kaestner KH, Bixby JL, Lemmon VP, and Goldberg JL, (2009). KLF family members regulate intrinsic axon regeneration ability. Science326, 298–301. [PubMed: 19815778]

Murai J, Zhang H, Pongor L, Tang S-W, Jo U, Moribe F, Ma Y, Tomita M, and Pommier Y, (2020). Chromatin Remodeling and Immediate Early Gene Activation by SLFN11 in Response to Replication Stress. Cell Rep. 30, 4137–4151.e6. [PubMed: 32209474]

Nix P, and Bastiani M, (2012). DLK: the “preconditioning” signal for axon regeneration?Neuron74, 961–963. [PubMed: 22726825]

Okuyama N, Kiryu-Seo S, and Kiyama H, (2007). Altered expression of Smad family members in injured motor neurons of rat. Brain Res. 1132,36–41. [PubMed: 17166487]

Painter MW, Brosius Lutz A, Cheng YC, Latremoliere A, Duong K, Miller CM, Posada S, Cobos EJ, Zhang AX, Wagers AJ, et al. (2014). Diminished Schwann cell repair responses underlie age-associated impaired axonal regeneration. Neuron 83, 331–343. [PubMed: 25033179]

Patodia S, and Raivich G, (2012). Role of transcription factors in peripheral nerve regeneration. Front. Mol. Neurosci5, 8. [PubMed: 22363260]

Raivich G, Bohatschek M, Da Costa C, Iwata O, Galiano M, Hristova M, Nateri AS, Makwana M, Riera-Sans L, Wolfer DP, et al. (2004). The AP-1 transcription factor c-Jun is required for efficient axonal regeneration. Neuron 43, 57–67. [PubMed: 15233917]

Renthal W, Tochitsky I, Yang L, Cheng Y-C, Li E, Kawaguchi R, Geschwind DH, and Woolf CJ, (2020). Transcriptional Reprogramming of Distinct Peripheral Sensory Neuron Subtypes after Axonal Injury. Neuron108, 128–144.e9. [PubMed: 32810432]

Saijilafu H, Hur EM, Liu CM, Jiao Z, Xu WL, and Zhou FQ, (2013). PI3K-GSK3 signalling regulates mammalian axon regeneration by inducing the expression of Smad1. Nat. Commun4, 2690. [PubMed: 24162165]

Sakasai R, and Iwabuchi K, (2016). The distinctive cellular responses to DNA strand breaks caused by a DNA topoisomerase I poison in conjunction with DNA replication and RNA transcription. Genes Genet. Syst90, 187–194. [PubMed: 26616758]

Sakuma M, Gorski G, Sheu SH, Lee S, Barrett LB, Singh B, Omura T, Latremoliere A, and Woolf CJ, (2016). Lack of motor recovery after prolonged denervation of the neuromuscular junction is not due to regenerative failure. Eur. J. Neurosci43, 451–462. [PubMed: 26332731]

Sapunar D, Modric-Jednacak K, Grkovic I, Michalkiewicz M, and Hogan QH, (2005). Effect of peripheral axotomy on pain-related behavior and dorsal root ganglion neurons excitability in NPY transgenic rats. Brain Res. 1063, 48–58. [PubMed: 16259969]

Schwer B, Wei PC, Chang AN, Kao J, Du Z, Meyers RM, and Alt FW, (2016). Transcription-associated processes cause DNA double-strand breaks and translocations in neural stem/progenitor cells. Proc. Natl. Acad. Sci. USA113, 2258–2263. [PubMed: 26873106]

Seijffers R, Allchorne AJ, and Woolf CJ, (2006). The transcription factor ATF-3 promotes neurite outgrowth. Mol. Cell. Neurosci32, 143–154. [PubMed: 16713293]

Seijffers R, Mills CD, and Woolf CJ, (2007). ATF3 increases the intrinsic growth state of DRG neurons to enhance peripheral nerve regeneration. J. Neurosci27, 7911–7920. [PubMed: 17652582]

Shanbhag NM, Evans MD, Mao W, Nana AL, Seeley WW, Adame A, Rissman RA, Masliah E, and Mucke L, (2019). Early neuronal accumulation of DNA double strand breaks in Alzheimer's disease. Acta Neuropathol. Commun7, 77. [PubMed: 31101070]

Sordet O, Redon CE, Guirouilh-Barbat J, Smith S, Solier S, Douarre C, Conti C, Nakamura AJ, Das BB, Nicolas E, et al. (2009). Ataxia telangiectasia mutated activation by transcription- and topoisomerase I-induced DNA double-strand breaks. EMBO Rep. 10, 887–893. [PubMed: 19557000]

Tedeschi A, Nguyen T, Puttagunta R, Gaub P, and Di Giovanni S, (2009). A p53-CBP/p300 transcription module is required for GAP-43 expression, axon outgrowth, and regeneration. Cell Death Differ. 16, 543–554. [PubMed: 19057620]

Thompson MR, Xu D, and Williams BR, (2009). ATF3 transcription factor and its emerging roles in immunity and cancer. J. Mol. Med. (Berl.)87, 1053–1060. [PubMed: 19705082]

Tsujino H, Kondo E, Fukuoka T, Dai Y, Tokunaga A, Miki K, Yonenobu K, Ochi T, and Noguchi K, (2000). Activating transcription factor 3 (ATF3) induction by axotomy in sensory and motoneurons: A novel neuronal marker of nerve injury. Mol. Cell. Neurosci15, 170–182. [PubMed: 10673325]

Van der Zee CE, Nielander HB, Vos JP, Lopes da Silva S, Verhaagen J, Oestreicher AB, Schrama LH, Schotman P, and Gispen WH, (1989). Expression of growth-associated protein B-50 (GAP43) in dorsal root ganglia and sciatic nerve during regenerative sprouting. J. Neurosci9, 3505–3512. [PubMed: 2552034]

van Kesteren RE, Mason MRJ, Macgillavry HD, Smit AB, and Verhaagen J, (2011).A gene network perspective on axonal regeneration. Front. Mol. Neurosci4, 46. [PubMed: 22125511]

Wang JC, (2002). Cellular roles of DNA topoisomerases: a molecular perspective. Nat. Rev. Mol. Cell Biol3, 430–440. [PubMed: 12042765]

Wang Z, Reynolds A, Kirry A, Nienhaus C, and Blackmore MG, (2015). Overexpression of Sox11 promotes corticospinal tract regeneration after spinal injury while interfering with functional recovery. J. Neurosci35, 3139–3145. [PubMed: 25698749]

Wei PC, Chang AN, Kao J, Du Z, Meyers RM, Alt FW, and Schwer B, (2016). Long Neural Genes Harbor Recurrent DNA Break Clusters in Neural Stem/Progenitor Cells. Cell164, 644–655. [PubMed: 26871630]

Weng YL, An R, Cassin J, Joseph J, Mi R, Wang C, Zhong C, Jin SG, Pfeifer GP, Bellacosa A, et al. (2017). An Intrinsic Epigenetic Barrier for Functional Axon Regeneration. Neuron 94, 337–346.e6. [PubMed: 28426967]

Yang X, Liu R, Xu Y, Ma X, and Zhou B, (2021). The Mechanisms of Peripheral Nerve Preconditioning Injury on Promoting Axonal Regeneration. Neural Plast. 2021, 6648004. [PubMed: 33505458]

Ziv NE, and Spira ME, (1995). Axotomy induces a transient and localized elevation of the free intracellular calcium concentration to the millimolar range. J. Neurophysiol74, 2625–2637. [PubMed: 8747220]

Highlights

- Axonal injury rapidly induces ATF3-dependent expression of RAGs in DRG neurons
- An ATF3 reporter is used to identify how ATF3 is induced in injured neurons
- Topo I inhibition increases ATF3 expression and enhances axonal regeneration
- DNA breaks are increased at the ATF3 locus in injured neurons by Topo I inhibition

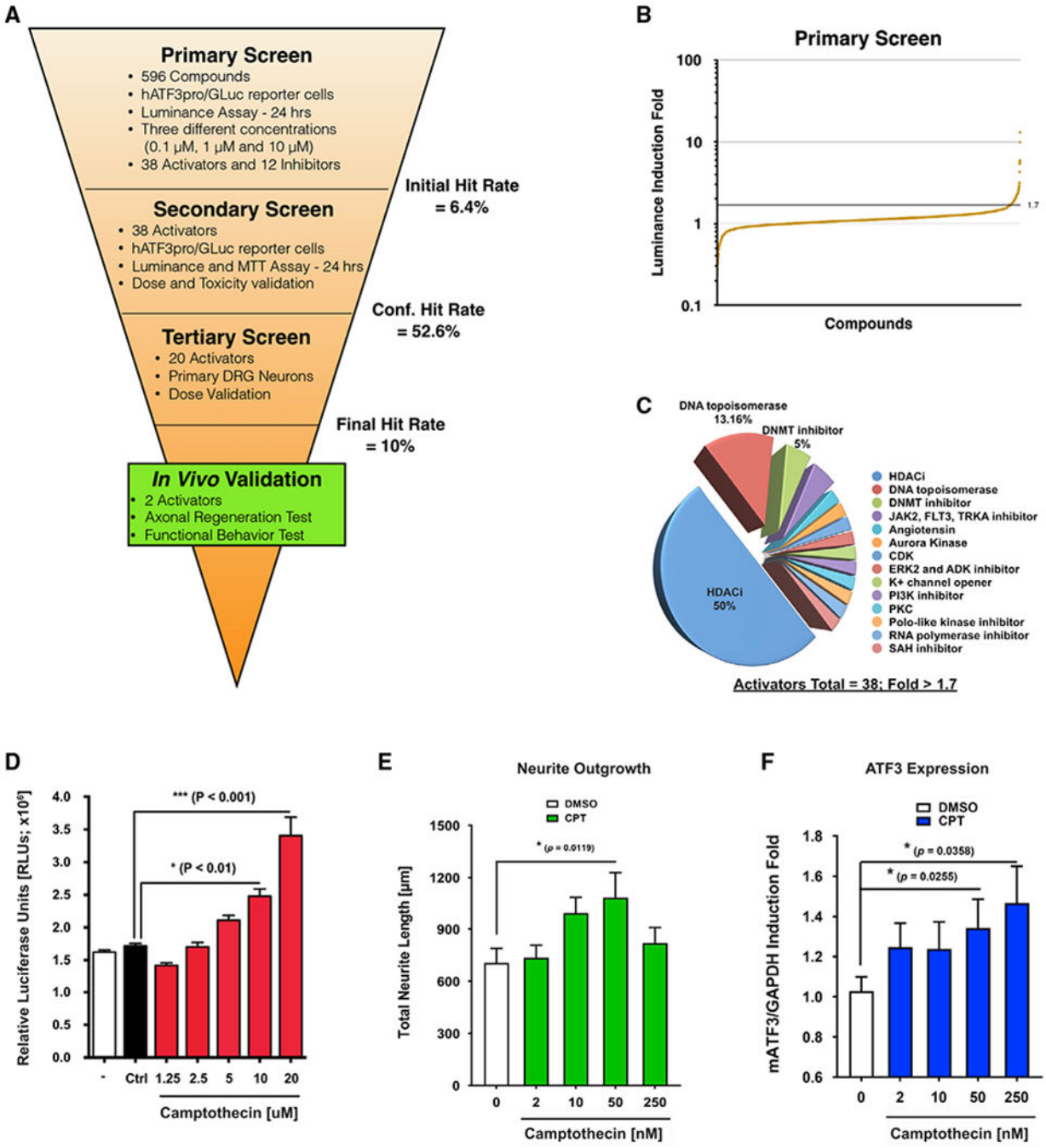

Figure 1. Phenotypic screen identifies TOP I inhibitor camptothecin as increasing ATF3 expression and enhancing neurite outgrowth

(A) Schematic representation of the phenotypic screen.

(B) Fold change in luminance for the 596 compounds tested in a *hATF3pro*/GLuc reporter line. The line at 1.7-fold indicates the cut-off threshold for hit identification.

(C) Distribution of annotated targets for the 38 activators identified by the primary screen.

(D) ATF3 induction in the hATF3/GLuc reporter line treated with different doses of CPT for 24 h.

(E) Neurite outgrowth of cultured primary DRG neurons after treatment with DMSO (white) or CPT (green).

(F) Effects of CPT on endogenous ATF3 expression in cultured primary DRG neurons. Expression of *mAtf3* was quantified by qPCR at 12 h after CPT stimulation. *$p < 0.05$; ***$p < 0.001$; unpaired t test, and one-way ANOVA with Fisher's least significant difference (LSD) test, Bonferroni's correction with multiple comparisons, Bartlett's correction. Data are represented as mean ± SEM.

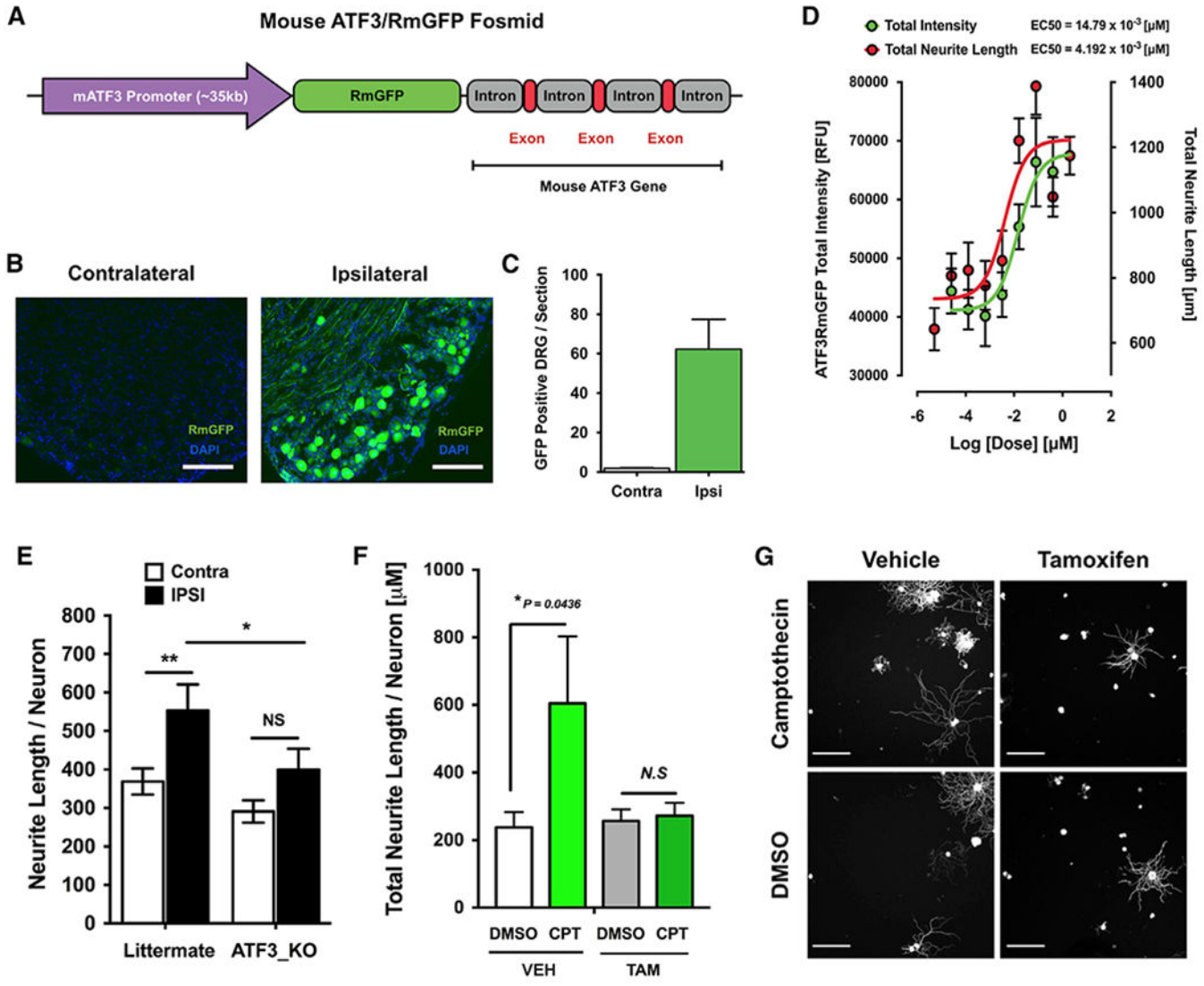

Figure 2. Camptothecin enhances neurite outgrowth by upregulation of ATF3 in primary DRG neurons

(A) Schematic representation of *mAtf3pro*/RmGFP reporter mouse comprising the 35-kb mouse *Atf3* promoter (purple), RmGFP reporter gene (green), and full mouse *Atf3* gene (red, exon; gray, intron).

(B) Representative images of ipsilateral and contralateral DRG of *mAtf3pro*/RmGFP reporter mouse 2 days after injury. Scale bar: 150 μm.

(C) Quantification of GFP-positive neurons in ipsilateral and contralateral DRG 2 days after sciatic nerve injury.

(D) The effect of CPT on RmGFP intensity and total neurite length in primary DRG neurons isolated from *mAtf3pro*/RmGFP reporter mice.

(E) Quantification of average neurite length of DRG neurons from *Brn3a::Atf3KO* mice 7 days after sciatic nerve injury.

(F) Effect of CPT (50 nM) on total neurite length in primary DRG neurons from *Brn3a::Atf3KO* mice with or without tamoxifen.

(G) Representative images of βIII-tubulin-positive DRG neurons from *Brn3a::Atf3KO* mouse after CPT or DMSO treatment with or without tamoxifen. Scale bar: 10 μm. NS, non-significant. *$p < 0.05$; **$p < 0.01$; one-way ANOVA with Fisher's LSD test, and unpaired two-tailed t test. Data are represented as mean ± SEM.

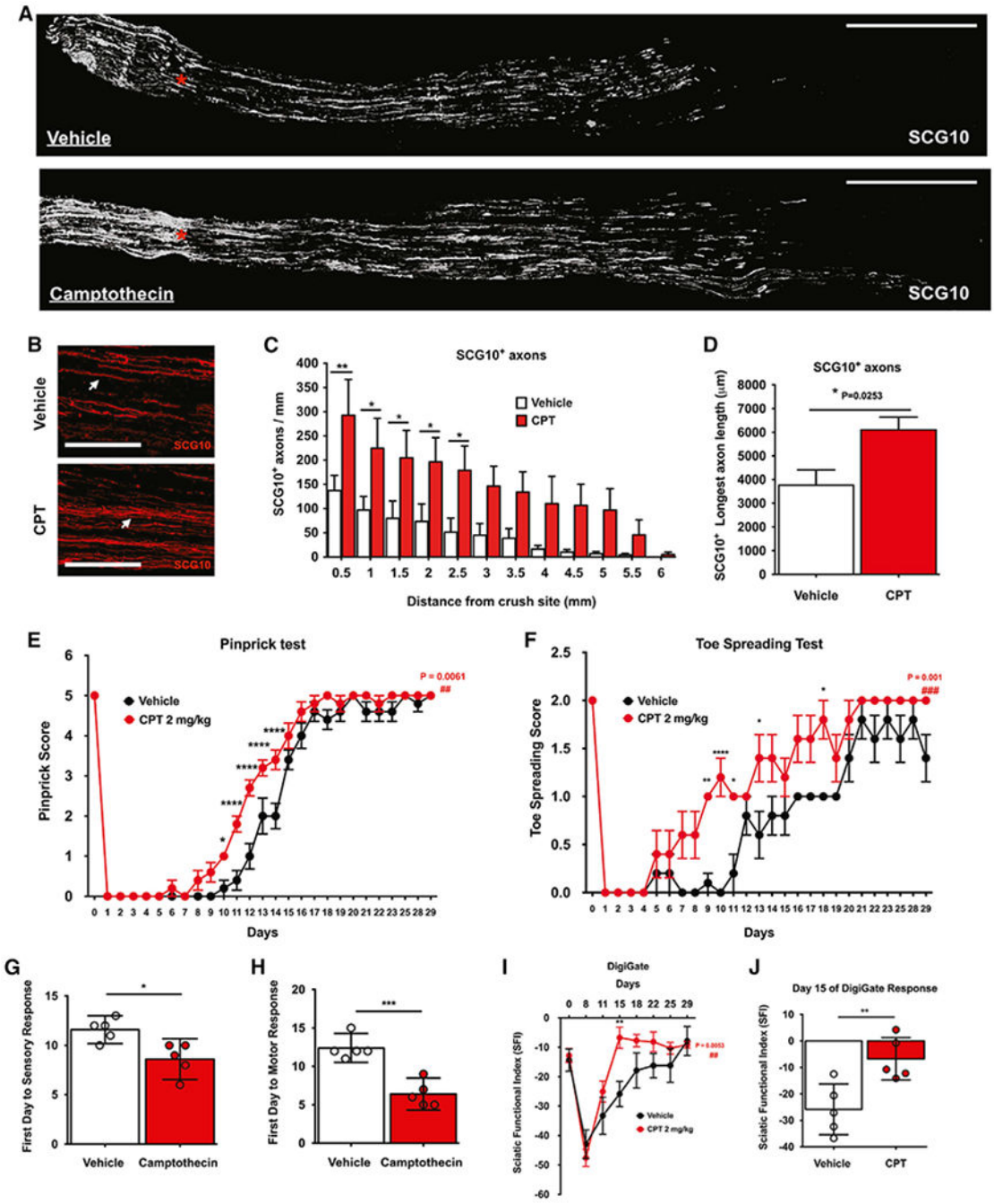

Figure 3. Camptothecin promotes axonal regeneration *in vivo* and accelerates functional recovery of neuron after sciatic nerve injury

(A) Representative images of the effect of CPT treatment on axonal regeneration following sciatic nerve crush. Regenerating axons stained for SCG10. Scale bar: 1 mm. Asterisks indicate crush site.

(B) High-magnification (20×) representative images of sciatic nerve sections from vehicle- and CPT-treated mice at ~1 mm distal from crush site. Arrows indicate single regenerating axons. Scale bar: 100 μm.

(C) Number of SCG10-stained axons at indicated distances from crush site 5 days after sciatic nerve crush.
(D) Average length of longest SCG10-labeled axons after sciatic nerve crush.
(E and F) Time course of sensory and motor functional recovery measured by pinprick (E) and toe spreading score (F).
(G and H) First day to a positive sensory (G) or motor (H) behavioral response.
(I) Motor functional recovery recorded by DigiGate.
(J) Sciatic functional index (SFI) tested 15 days after sciatic nerve crush. *$p < 0.05$; **$p < 0.01$; ***$p < 0.001$; ****$p < 0.0001$; two-way ANOVA with Bonferroni multiple comparisons test, Fisher's LSD test, and unpaired two-tailed t test. Data are represented as mean ± SEM; n = 5 mice per cohort.

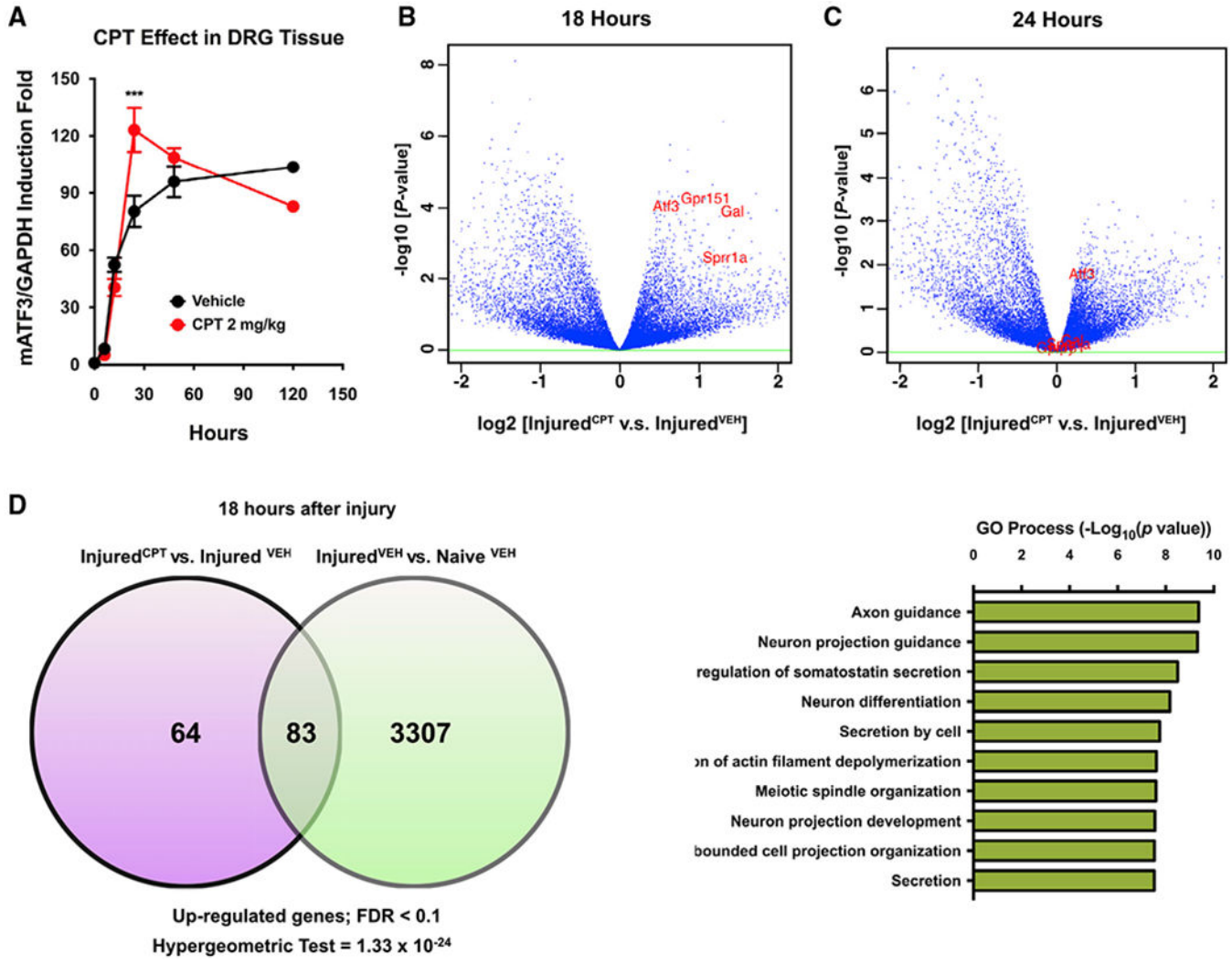

Figure 4. Effect of camptothecin on RNA-seq profiling of injured DRGs

(A) Quantitative PCR analysis of ATF3 expression in injured DRGs after CPT treatment.

(B and C) Volcano plots representing RNA-seq profiles of Injury^{CPT} versus Injury^{VEH} DRGs at 18 (B) and 24 h (C) (n ≥ 3 per group) post-injury. *Atf3, Sprr1a, Gal*, and *Gpr151* are indicated.

(D) Venn diagram depicting overlapping upregulated genes between Injury^{CPT} versus Injury^{VEH} and Injury^{VEH} versus Naive^{VEH} 18 h after injury.

(E) Gene Ontology enrichment scores of overlapping upregulated genes by MetaCore analysis. ***p < 0.001, one-way ANOVA with Fisher's LSD test. Data are represented as mean ± SEM.

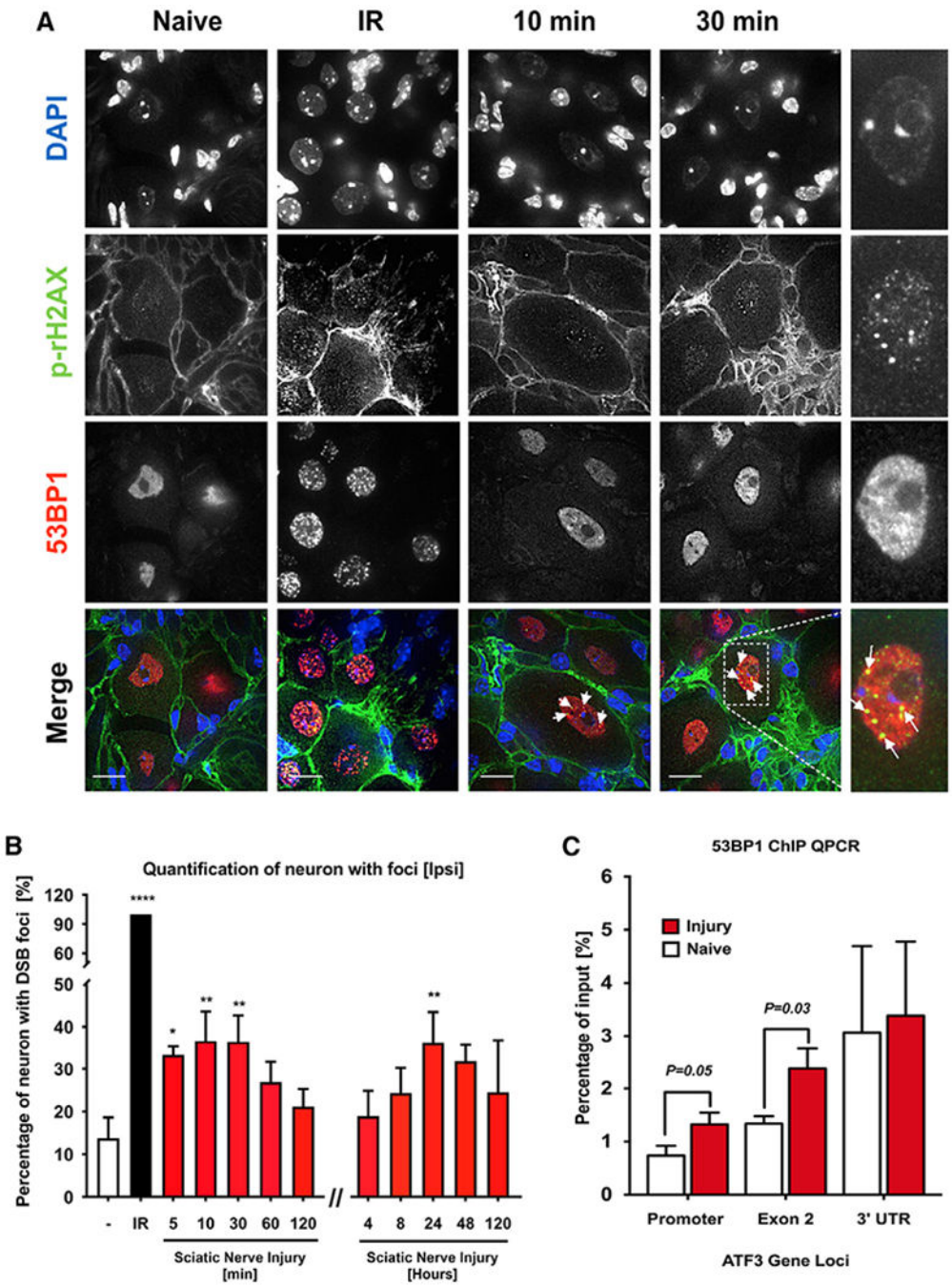

Figure 5. Transient DNA breaks occur at ATF3 locus after injury to induce ATF3 expression in primary DRG neuron

(A) γ-H2AX and 53BP1 staining in naive DRG and in DRGs at 10 and 30 min after a sciatic nerve injury. DRGs from a mouse exposed to irradiation (IR) for 30 min were included as a positive control for DNA double-strand breaks (DSBs). Arrowheads indicate γ-H2AX and 53BP1 double-positive foci. Scale bar: 10 μm.

(B) Quantification of average γ-H2AX and 53BP1 double-positive foci/DRG at different times post-sciatic nerve injury.

(C) Quantitative PCR analysis of 53BP1 ChIP across the ATF3 locus in naive and injured DRGs. *$p < 0.05$, **$p < 0.01$, one-way ANOVA with Fisher's LSD test, and unpaired two-tailed t test. Data are represented as mean ± SEM.

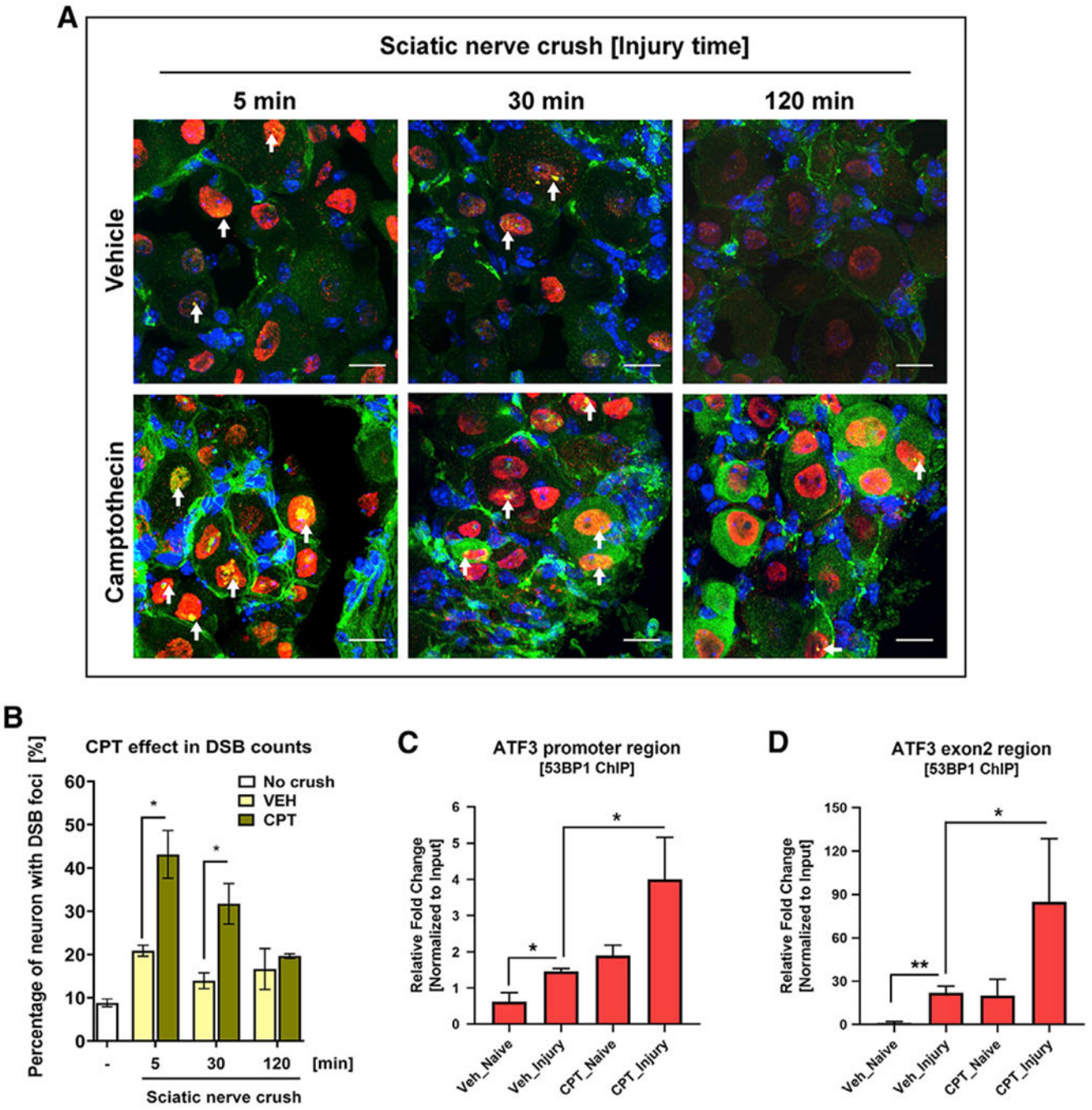

Figure 6. Camptothecin increases DNA breaks at ATF3 locus in DRG neurons after sciatic nerve injury

(A) *In vivo* compound treatment in mice at 30 min prior to nerve injury. γ-H2AX and 53BP1 staining in injured DRG at 5, 10, and 30 min after a sciatic nerve crush. Arrowheads indicate γ-H2AX and 53BP1 double-positive foci. Scale bar: 10 μm.

(B) Quantification of percentage of DNA breaks per CPT- or vehicle-treated DRG at different time points post-sciatic nerve crush.

(C and D) Quantitative PCR analysis of 53BP1 ChIP across the ATF3 promoter locus (C) and ATF3 exon 2 locus (D) in CPT- or vehicle-treated injured DRGs. *$p < 0.05$, **$p < 0.01$,

one-way ANOVA with Sidak comparisons test, and unpaired t test. Data are represented as mean ± SEM.

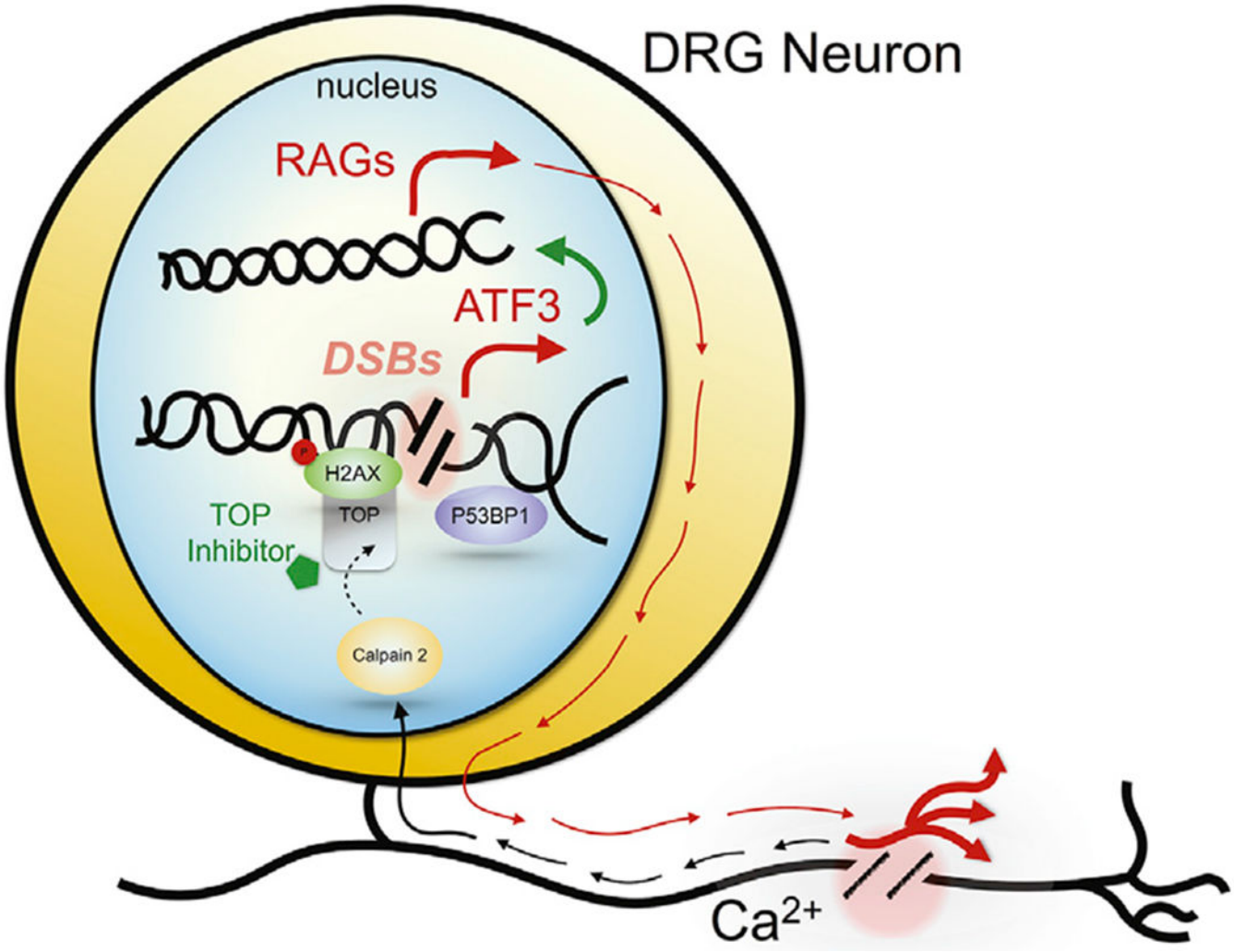

Figure 7. Proposed model for the role of DNA double-strand breaks (DSBs) in inducing ATF3 activation and driving the regeneration program after nerve injury

After sciatic nerve injury, calcium influx at the site of injury occurs and initiates a calcium wave that moves retrogradely to the neuronal soma to activate calpain-2, a proteolytic enzyme. Activated calpain-2 truncates topoisomerase I (TOP I) to impair its DNA re-ligation activity, an effect similar to TOP I inhibitors. This leads to DNA breaks at the ATF3 gene locus. DNA breaks occurring at the ATF3 gene locus ease the torsional stress of entangled DNA segments and free the stalled polymerase to produce a burst of ATF3 transcription. Induction of ATF3 drives expression of downstream regeneration-associated genes (RAGs) that enable axonal regeneration.

KEY RESOURCES TABLE

REAGENT or RESOURCE	SOURCE	IDENTIFIER
Antibodies		
Mouse beta-tubulin III antibody	Sigma	Cat# T8578; RRID: AB_1841228
Rabbit anti-ATF3 antibody (C-19)	Santa Cruz	Cat# SC-188; RRID:AB_2258513
Rabbit anti-GAPDH antibody (HRP conjugated)	Cell Signaling	Cat# 8884; RRID:AB_11129865
SCG10 antibody	Novus	Cat# NBP1-49461; RRID:AB_10011569
phosph-H2AX antibody (Ser139)	Millipore	Cat# 05-636; RRID:AB_309864
53BP1 antibody	Novus	Cat# NB100-304; RRID:AB_10003037
TRPV1 antibody	Alomone	Cat# ACC-030; RRID:AB_2313819
NF200 antibody	Millipore	Cat# AB5539; RRID:AB_11212161
DyLignt_594 conjugated Isolectin B4 antibody	VectorLab	Cat# DL-1207
Laminin-gamma antibody	Millipore	Cat# MAB-1914P; RRID:AB_1587233
Bacterial and virus strains		
One Shot Stbl3 chemically competent *E. coli*	Thermo Fisher	Cat# C737303
Chemicals, peptides, and recombinant proteins		
Camptothecin	Sigma	Cat# C9911
Tamoxifen	Sigma	Cat# T5648
Complete Mini, EDTA-free (proteinase inhibitor cocktail)	Sigma	Cat# 11836170001
Chaetocin	Tocris	Cat# 4504
Trichostatin A	Tocris	Cat# 1406
Mounting medium with DAPI	VectorLab	Cat# H1200
Critical commercial assays		
CellTiter 96® Non-Radioactive Cell Proliferation Assay (MTT)	Promega	Cat# G4000
Pierce Gaussia Luciferase Glow Assay Kit	ThermoFisher	Cat# 16161
Deposited data		
RNA-seq data	This paper	GSE113672
Experimental models: Cell lines		
hATF3pro/GLuc reporter cell line	This paper	N/A
Experimental models: Organisms/strains		
mAtf3pro/RmGFP mouse model	This paper	N/A
Atf3 flox/flox mouse model	This paper	N/A
Brn3a-Cre^{ERT2}::*Atf3* flox/flox mouse model	This paper	N/A
Oligonucleotides		
Real-time PCR primers	IDT	Table S3
Recombinant DNA		
hATF3pro/Gluc Fosmid	This paper	N/A
mATF3/RmGFP Fosmid	This paper	N/A
Software and algorithms		

REAGENT or RESOURCE	SOURCE	IDENTIFIER
Cellomics scan	Thermo Fisher	https://www.thermofisher.com/us/en/home/technical-resources/software-downloads.html#cell-imaging-hcs
Prism	GraphPad	https://www.graphpad.com/scientific-software/prism/
NIS-ElementsAR	Nikon	https://www.nikon.com/products/microscope-solutions/support/download/software/imgsfw/nis-ar_v43001du164.htm
MetaCore pathway analysis	Clarivate	https://portal.genego.com/
BioRender	BioRender.com	https://biorender.com/
Fiji	ImageJ	RRID:SCR_002285
Adobe Illustrator CC	Adobe Systems	RRID: SCR_010279